Research Square

Preprints are preliminary reports that have not undergone peer review.
They should not be considered conclusive, used to inform clinical practice,
or referenced by the media as validated information.

The vaginal microbiome associates with increased vaccine immune responses in the RV306 HIV vaccine trial in Thai women

Leighanne Main

lrm91@case.edu

Case Western Reserve University

Alessandra Borgognone

IrsiCaixa, AIDS Research Institute https://orcid.org/0000-0001-5487-3016

Matthew Hale

US Military HIV Research Program, Walter Reed Army Institute of Research

Rasmi Thomas

Walter Reed Army Institute of Research https://orcid.org/0000-0002-2116-2418

Francesc Català-Moll

IrsiCaixa AIDS Research Institute https://orcid.org/0000-0002-2354-8648

Samantha Knodel

Case Western Reserve University

Laura Noel-Romas

Case Western Reserve

Riley Hall

Case Western Reserve University

Samantha Bailey

Case Western Reserve University

Mariona Parera

IrsiCaixa & AIDS Unit, Hospital Universitari Germans Trias i Pujol, Universitat Autònoma de Barcelona, Badalona

Ashley Yoon

Case Western Reserve University

Sausan Azzam

Case Western Reserve University

Oriol Careta

irsicaixa https://orcid.org/0000-0003-1333-0300

Maria Casadellà

IrsiCaixa AIDS Research Institute, Hospital Universitari Germans Trias I Pujol, Badalona, Barcelona, Spain. https://orcid.org/0000-0002-4115-2305

Oluwatobiloba Taylor
Case Western Reserve University

Siriwat Akapirat
Case Western Reserve University

Sorachai Nitayaphan
Armed Forces Research Institute of Medical Sciences

Suwat Chariyalertsak
Research Institute for Health Sciences (RIHES), Chiang Mai University, Chiang Mai, Thailand

Punnee Pitisuttithum
Mahidol University https://orcid.org/0000-0003-3215-2183

Surawach Rittiroongrad
WRAIR-Armed Forces Research Institute of Medical Sciences, Bangkok, Thailand

Julie Ake
United States Military HIV Research Program https://orcid.org/0000-0003-3831-5828

Sandhya Vasan
Walter Reed Army Institute of Research

Carolina Herrera
CONRAD, Eastern Virginia Medical School, Macon & Joan Brock Virginia Health Sciences at Old Dominion University

Roger Paredes
IrsiCaixa https://orcid.org/0000-0002-6553-691X

Alexandra Schuetz
Department of Retrovirology, Armed Forces Research Institute of Medical Sciences, United States Component, Bangkok

Adam Burgener
Case Western University

Article

Keywords:

Posted Date: November 19th, 2026

DOI: https://doi.org/10.21203/rs.3.rs-11706184/v1

License: This work is licensed under a Creative Commons Attribution 4.0 International License.
Read Full License

Additional Declarations: There is **NO** Competing Interest.

Title: The vaginal microbiome associates with increased vaccine immune responses in the RV306 HIV vaccine trial in Thai women

Author list:

Leighanne R Main[1], Alessandra Borgognone[2], Matthew Hale[3,4], Rasmi Thomas[4], Francesc Català-Moll[2], Samantha Knodel[1,5], Laura Noel-Romas[1,5], Riley Hall[1], Samantha Bailey[1], Mariona Parera[2], Ashley Yoon[1], Sausan Azzam[1], Oriol Careta[2], Maria Casadella[2], Oluwatobiloba Taylor[1], Siriwat Akapirat[6], Sorachai Nitayaphan[6], Suwat Chariyalertsak[7], Punnee Pitisuttithum[8], Surawach Rittiroongrad[6], Julie A Ake[4], Sandhya Vasan[3,4], Carolina Herrera[9], Roger Paredes[1,2,10], Alexandra Schuetz[3,6,8], Adam D. Burgener[1,5,10] and the RV306 study group[11]

Corresponding Author: Leighanne R Main (lrm91@case.edu)

1. Center for Global Health and Diseases, Department of Pathology, Case Western Reserve University, Cleveland, OH, USA
2. IrsiCaixa, Badalona, Catalonia, Spain
3. Henry M. Jackson Foundation for the Advancement of Military Medicine, Inc, Bethesda, MD, USA
4. US Military HIV Research Program, Walter Reed Army Institute of Research, Silver Spring, MD, USA
5. Department of Obstetrics, Gynecology and Reproductive Sciences, Case Western Reserve University, Cleveland, OH, USA
6. WRAIR-Armed Forces Research Institute of Medical Sciences, Bangkok, Thailand
7. Research Institute for Health Sciences (RIHES), Chiang Mai University, Chiang Mai, Thailand
8. Vaccine Trial Centre, Faculty of Tropical Medicine, Mahidol University, Bangkok, Thailand
9. CONRAD, Eastern Virginia Medical School, Macon & Joan Brock Virginia Health Sciences at Old Dominion University, Norfolk, VA, USA
10. Department of Infectious Diseases, Hospital Germans Trias i Pujol, Badalona, Catalonia, Spain
11. A full list of members and their affiliations appears at the end of the paper.

Abstract:

Background: The microbiome has been implicated in host immunity, but its relationship to vaccine-induced mucosal responses in the female genital tract is not well understood. Here we compared vaginal microbiome composition to host immunity and humoral immune responses to an HIV vaccine.

Methods: Vaginal microbiome data was generated from participants receiving the RV144 ALVAC-HIV/AIDSVAX B/E prime/boost vaccine in the RV306 trial, and compared to mucosal and systemic immunity and binding antibody (bAb) levels at 2 weeks post-vaccine regimen.

Results: Participants with *Lactobacillus* dominant microbiomes associated with increased mucosal and systemic bAb levels compared to non-*Lactobacillus* microbiomes. Pathways enriched in high vaccine responders and *Lactobacillus* dominant participants included increased mucosal innate immunity and systemic adaptive and B -cell responses, while non-*Lactobacillus* microbiomes associated with increased mucosal and systemic inflammatory phenotypes.

Conclusion: These data suggest an association between increased innate immunity, *Lactobacillus*-dominant microbiome, and increased vaccine-induced bAb responses, which could inform improved interventional strategies.

Introduction

The development of an effective vaccine against the Human Immunodeficiency Virus (HIV) remains a major global health priority, with HIV affecting over 40 million people worldwide, including approximately 1.2 million in the US, with around 32,000 new infections every year.[1] The HIV vaccine field has faced largely disappointing results, including the HVTN505 and STEP trials, which evaluated DNA/rAd5 and MRKAd5 HIV-1 gag/pol/nef vaccine regimens, respectively, with both trials failing to demonstrate efficacy.[2,3] Numerous other trials have also been conducted, but none have successfully advanced through all phases of clinical development.[4–6] The RV144 trial in Thailand, using an ALVAC-HIV.AIDSVAX B/E prime/boost regimen provided the first evidence of vaccine-induced protection, demonstrating a modest efficacy of 31.2% after three years.[7,8] However, this level of protection remains insufficient for large-scale implementation. These outcomes highlight a critical gap in understanding the mechanisms underlying protective immunity.

HIV transmission primarily occurs across mucosal surfaces, including the vaginal, rectal, and penile epithelium during sexual exposure. The microbiome plays a critical role in maintaining homeostasis at these sites.[9,10] For example, *Lactobacillus* species, considered a hallmark species of a healthy female reproductive tract, produce fermentation by-products such as lactic acid, which help maintain an acidic pH, thus deterring opportunistic pathogens.[11,12] Not surprisingly, an altered vaginal microbiome has been linked to many reproductive health outcomes, including pre-term birth, endometriosis, STI acquisition (including HIV), amongst others.[13–16] Vaginal microbiome dysbiosis, or bacterial vaginosis (BV), associates with changes in host immune functions at mucosal surfaces, including increased pro-inflammatory cytokines, increased numbers of activated immune cells such as CD4+ T-cells, and epithelial barrier disruption.[9,10,17] Notably, even asymptomatic BV can induce similar immunological changes.[17] These alterations have been consistently associated with increased susceptibility to HIV acquisition, with some studies reporting up to a 6.7-fold increase in risk.[13,18–20] Despite these associations, the mechanisms by which the vaginal microbiome shapes mucosal immunity and barrier function remain poorly understood. Perhaps more importantly, it also remains widely unknown how the microbiome may affect HIV prevention strategies designed to induce mucosal immune responses, such as HIV vaccines.

Previous studies have focused on identifying immune correlates of protection and host factors that shape vaccine responsiveness, identifying IgG binding to the HIV V1V2 region as inversely correlated with HIV infection and IgA Env binding as predictive of infection,[21] as well as a modulatory effect on HIV acquisition by certain HLA class II genotypes.[22]

However, greater insight into potential mucosal immune correlates of protection, as well as host and environmental factors influencing vaccine responses, will be essential to improving the efficacy of future HIV vaccine trials.

Growing evidence suggests that the microbiome influences immune responses to vaccination.[23–26] Prior studies have demonstrated that variation in microbial composition can either enhance or diminish vaccine responses, including effects mediated by antibiotic exposure and baseline microbial diversity.[24–26] Microbial products themselves can also shape immunity; for example, bacterial flagellin has been shown to enhance antibody responses through innate immune activation.[27] During acute infection, dominant antibody responses during HIV-1 infection are directed toward non-neutralizing epitopes on the gp41 transmembrane protein, which are cross-reactive with commensal gut bacteria.[28] This phenomenon may divert immune responses away from protective targets, highlighting the potential for the microbiome to modulate vaccine efficacy.

In this study, we assessed the relationship between the female genital microbiome and vaccine-induced antibody responses in participants from the RV306 HIV vaccine clinical trial – a follow-up to the RV144 trial with additional booster vaccinations. Using an integrated multi-omic approach, we characterized vaginal microbial communities and their relationship to systemic immunity and vaccine immune responses. By integrating microbial and host immune data, we show that *Lactobacillus* dominant microbiomes associate with increased innate and adaptive immune responses and increased mucosal immune response, suggesting the vaginal microbiome may be a biomarker of elevated vaccine-induced immunity.

Results

Study Population

The RV306 HIV Vaccine Trial evaluated systemic and mucosal immune responses to an ALVAC-HIV (vCP1521) prime and AIDSVAX B/E boost regimen in healthy women from Thailand at three study sites – The Vaccine Trial Centre at Mahidol University and the Royal Thia Army in Bangkok, and the Research Institute for Health Sciences (RIHES) in Chiang Mai. Participants were randomized into four vaccine groups comprising the original RV144 regimen without a late boost or one of three late-boost regimens (ALVAC-HIV plus AIDSVAX B/E, AIDSVAX B/E alone, or ALVAC alone), with each group including a placebo subset.[29–31] For the present analyses, longitudinal vaginal CVM samples were available from 97 participants across three study visits (V0, V4, and V6), with complete microbiome data

available for 92 participants. Baseline demographic characteristics are summarized in Table 1.

Table 1. Cohort Demographics

	All participants	Lactobacillus dominant (LD)	Non-Lactobacillus dominant (nLD)
Average Age	29.27	29.56	28.97
Study Site Location			
Bangkok	90 (92.8%)	58 (93.5%)	30 (90.9%)
Chaing Mai (RIHES)	7 (7.2%)	4 (6.5%)	3 (9.1%)
Study Arm			
Vaccine	88 (90.7%)	54 (87.1%)	32 (97.0%)
Placebo	9 (9.3%)	8 (12.9%)	1 (3%)
Education			
Primary School	12 (12.4%)	9 (14.5%)	3 (9.1%)
Vocational	20 (20.6%)	12 (19.3%)	8 (24.2%)
Secondary School	53 (54.6%)	36 (58.1%)	17 (51.5%)
Bachelor's degree	10 (10.3%)	5 (8.1%)	5 (15.2%)
Occupation			
No occupation	18 (18.6%)	9 (14.5%)	9 (27.3%)
Student	6 (6.2%)	3 (4.8%)	3 (9.1%)
Merchant/Self-employed	20 (20.6%)	15 (24.2%)	5 (15.2%)
Employee	45 (46.4%)	31 (50.0%)	14 (42.3%)
Government employee	6 (6.2%)	4 (6.5%)	2 (6.1%)

Table 1 – Baseline demographics and clinical information of RV306 study participants in the vaginal microbiome study. Demographic information for all participants as well as LD and nLD subgroups of individuals. Age, study site, active (vaccine) or placebo study arm, highest level of education obtained, and occupation are provided below.
*Demographic data for two participants in this group was not available.

Microbiome Classification and Stratification

At baseline, vaginal microbiome profiling revealed distinct community structures across participants using both metagenomic and metaproteomic analysis. Metagenomic analysis

detected 254 taxa (genus species), while metaproteome analysis identified 22 taxa (genus species), with the highest abundance taxa including *L. iners (37%), L. crispatus (15%), Gardnerella* spp. *(15%),* other *Lactobacillus* spp. *(12%), Prevotella* spp. *(6.3%), and Megasphaera* spp. *(5.7%)* (Fig. 1A, Supplemental Fig. 1A). Based on metagenomic and metaproteomic analysis, participants were first classified as Lactobacillus-dominant (LD) or non-dominant (nLD) according to relative Lactobacillus abundance. Concordance between metaproteomic and metagenomic classification was 87.4% for LD/nLD assignment. Within these groups, community state type (CST) classification identified 42.1% (n = 40) of participants as *Lactobacillus iners*–dominant, 21.1% (n = 20) as *Lactobacillus crispatus*–dominant, and 36.8% (n = 35) with a non-*Lactobacillus* dominant polymicrobial microbiome with no predominant taxa, containing *G. vaginalis*, *Atopobium*, *Prevotella*, *Megasphaera*, and others (Fig. 1B, Supplemental Fig. 1B).

Alpha diversity was significantly lower in LD compared with nLD microbiomes (metagenomic mean Shannon H = 2.814 vs 3.331, p = 7.5×10^{-5}; metaproteomic mean Shannon H = 0.8636 vs 1.2473, p = $2.0 \times 10^{-}4$; Fig. 1C,G). Beta diversity, assessed via Bray–Curtis distances and visualized by principal coordinates analysis (PCoA), demonstrated clear clustering by LD status (metagenomic PERMANOVA p = 0.001; metaproteomic PERMANOVA p = 0.001, Fig. 1D,H). Interestingly, within CSTs, *L. iners*–dominant microbiomes exhibited the lowest alpha diversity in metaproteomic data but not by metagenomic sequencing (mean metagenome Shannon H = 3.109; mean metaproteome Shannon H = 0.6852), followed by *L. crispatus*–dominant (mean metagenomic Shannon H = 2.463; mean metaproteomic Shannon H = 1.0198), and polymicrobial CSTs had the highest diversity (mean metagenome Shannon H = 3.331; mean metaproteome Shannon H = 1.2614; Fig. 1E,I). PCoA of beta diversity similarly revealed distinct clustering by CST (metagenomic PERMANOVA p = 0.001; metaproteomic PERMANOVA p = 0.001, Fig. 1F,J). Microbiome composition did not differ by study site (alpha diversity p = 0.322; beta diversity p = 0.191) or treatment arm (alpha diversity p = 0.215; beta diversity p = 0.652).

Because the metaproteome reflects active microbial function through expressed protein products, metaproteomic LD/nLD classifications were used for primary downstream analyses of vaccine and host immune responses, with metagenomic classifications used for validation of key findings.

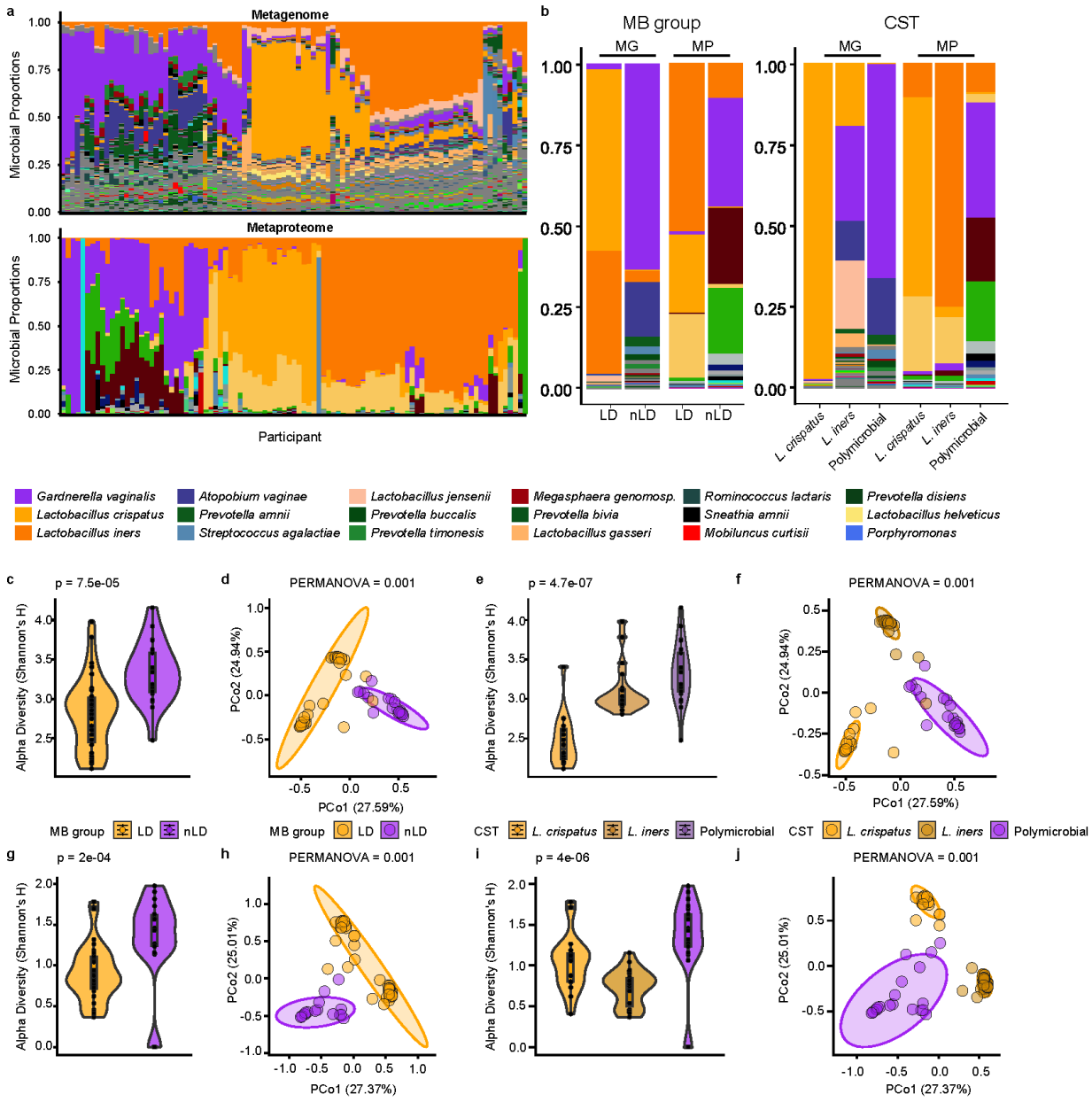


Figure 1 – Vaginal microbiome composition of study participants from the RV306 HIV vaccine trial. Vaginal microbiome composition was determined using both shotgun metagenomics and metaproteomics. (A) Heatmap of microbiome composition as shown by metagenomics (top) and metaproteomics (bottom) for all subjects at initial visit. Bray-Curtis distances of taxa were used to identify microbiome composition. (B) Overall microbiome composition as determined by metagenomic and metaproteomic data between LD vs. nLD subjects and CST groups at initial visit. Based on metagenomic classifications, alpha (C) and beta (D) diversity are shown between LD (orange) and nLD (purple) microbiome groups. Also shown are alpha (E) and beta (F) diversity between

different CSTs. Based on metaproteomic classifications, alpha (G) and beta (H) diversity for LD and nLD as well as alpha (I) and beta (G) diversity for CST groups based on are also shown.

Vaginal Microbiome Profiles are Largely Maintained Following Booster Vaccination

Longitudinal analysis revealed the majority (n = 61; 62.89%) of participants maintained stable microbiome classifications across all three timepoints for both the vaccine arm and placebo arm (Fig. 2A-B). Of these 61 participants, which included placebo arm individuals, with consistent microbiomes, 43 were consistently LD (LD→LD→LD) and 18 were consistently nLD (nLD→nLD→nLD). Longitudinal alpha diversity analyses within these stable groups showed no significant changes over time, with Kruskal–Wallis p-values of 0.61 for LD and 0.57 for nLD (Fig. 2C). Among CSTs, longitudinal alpha diversity was also stable (*L. crispatus*: p = 0.70; *L. iners*: p = 0.21; polymicrobial: p = 0.43; Fig. 2D). Beta diversity analyses confirmed clustering by LD status and CST rather than by study visit (LD PERMANOVA p = 0.001; CST PERMANOVA p =0.001, Fig. 2E-F), and no global shifts in microbiome composition over time were observed. These findings indicate that microbiome classifications were generally stable over the study period, supporting their use for downstream analyses of diversity, antibody responses, and transcriptomic associations.

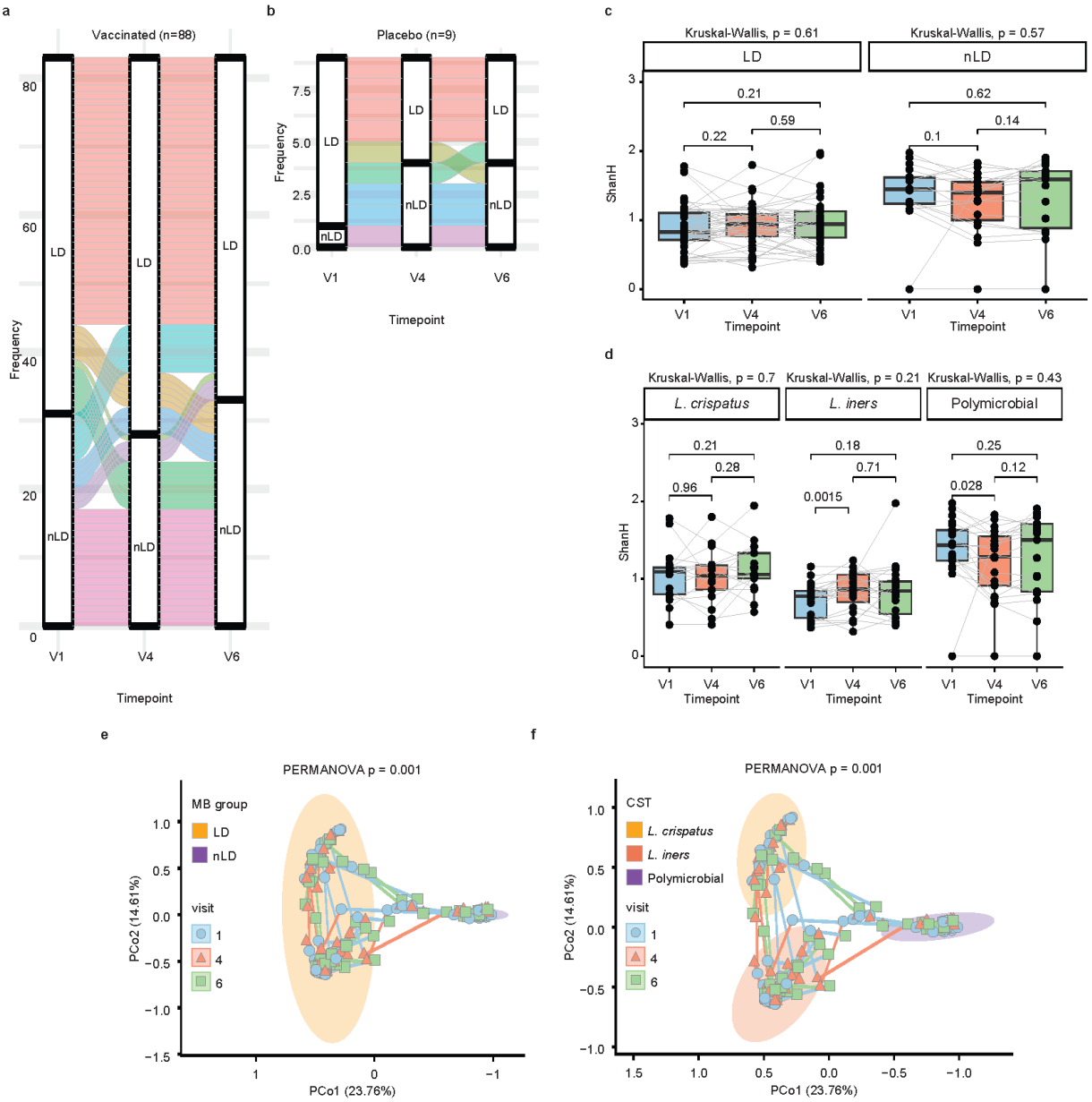


Figure 2 – Longitudinal stability and diversity of LD status during follow-up visits of RV306 study participants. Alluvial plots demonstrating changes in LD status over 3 visits for sample ascertainment for vaccinated (A) and placebo (B) individuals. Colors show either the stability of LD or nLD status, or the changes between these two statuses. Alpha diversity examined longitudinally across all visits are seen for both LD status (C) and CST status (D). Beta diversity changes over time were also examined for LD status (E) or CST (F).

Higher Levels of Systemic and Mucosal Binding Antibodies were Observed in Vaccine Recipients with LD Microbiomes

Within the RV144 ALVAC-HIV/AIDSVAX B/E regimen, vaccination induced robust HIV Env-specific binding antibody (bAb) responses in plasma, including gp120- and V1V2-directed antibodies, with HIV Env-specific IgG responses also observed in cervicovaginal mucus.[30,31] On account of this, we evaluated the relationship between vaccine-induced systemic and mucosal humoral responses and vaginal microbiome stratified by women with LD and nLD vaginal microbiomes. Of the 23 bAbs measured by ELISA, vaccine recipients with LD vaginal microbiomes displayed significantly higher bAb levels for IgG to gp120 A244.D11 ($p = 0.015$, Fig. 3A) and IgG to gp70 V1V2 92TH023 ($p = 0.004$, Fig. 3B) in plasma, and IgG to gp120 A244gD-D11 ($p = 0.039$, Fig. 3C) in vaginal mucosa. To further validate these findings, we also utilized metagenomic characterization of LD status (Supplemental Fig. 2A-C). When stratified by CST, no significant differences were observed (Supplemental Fig. 2D-F). No other antibodies examined displayed significant differences when stratified by LD status (Supplemental Fig. 3A) or CST (Supplemental Fig. 3B) for plasma or mucosa (LD status, Supplemental Fig. 4A; CST, Supplemental Fig. 4B).

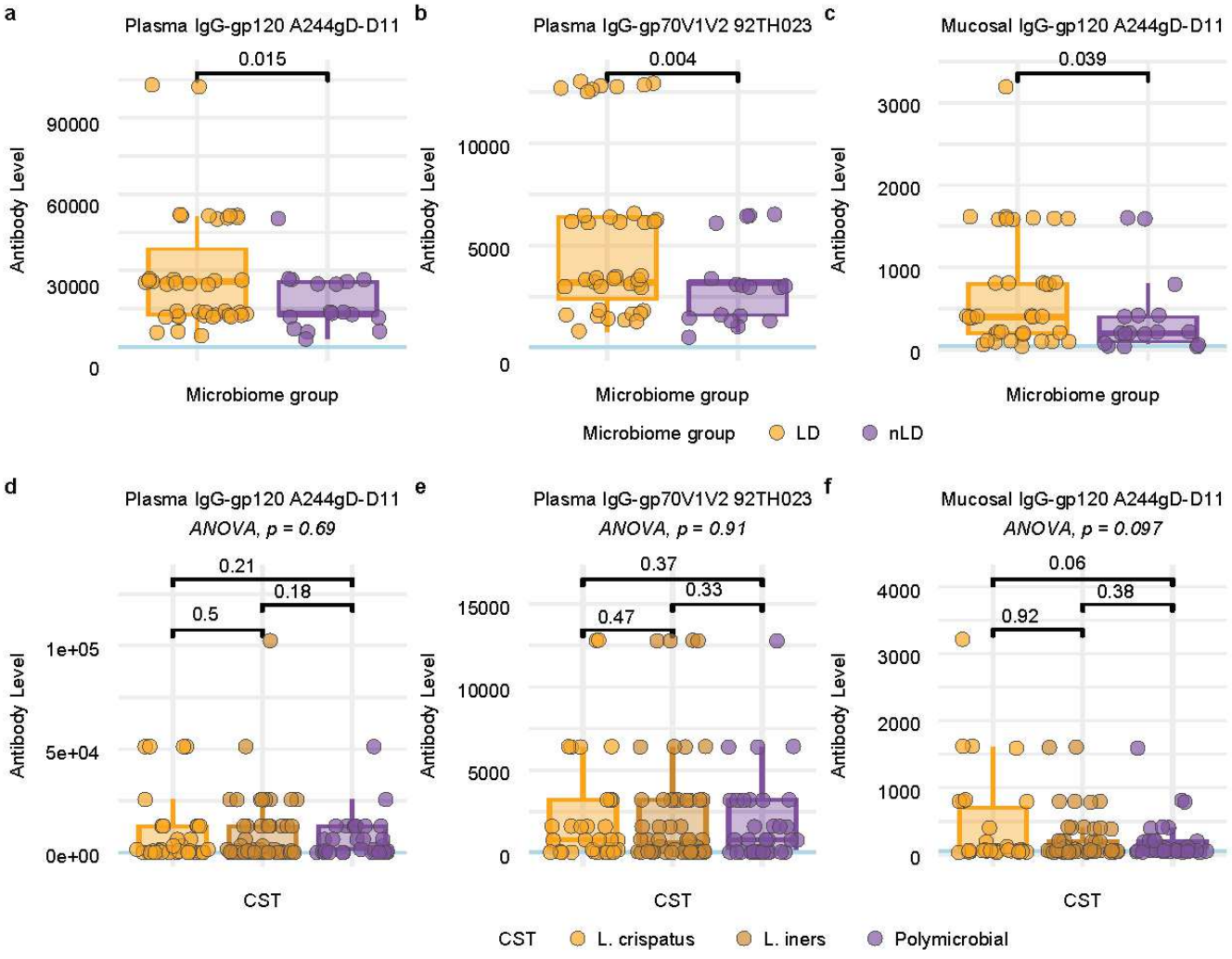


Figure 3 – Relationship between baseline vaginal microbiome composition and HIV vaccine binding antibody titer at 26 weeks post vaccination. Antibody levels measured in plasma and vaginal mucosa were compared between individuals with LD (orange) and nLD (purple) vaginal microbiomes, where IgG-gp120 A244gD-D11 in plasma (A), IgG-gp70V1V2 92TH023 in plasma (B), and Ig-gp120 A244-D11 in mucosa (C) were higher in the LD group. The LD group had more medium to high responders in all three antibodies compared to nLD. Stratifications are also shown based on CST are shown for IgG-gp120 A244gD-D11 in plasma (D), IgG-gp70V1V2 92TH023 in plasma (E), and Ig-gp120 A244-D11 in mucosa (F).

LD microbiomes associate with increased mucosal innate and adaptive immune signatures in mass spectrometry

Mass spectrometry of cervicovaginal samples identified 861 human proteins in the mucosal and plasma proteome. Participants were stratified by antibody responder status (high vs low, tertiles; non-responders grouped with low; see methods) and by microbiome classification (LD vs nLD). Differential protein abundance analyses identified significant associations ($p < 0.05$) for 175 proteins with high antibody responders and 178 proteins with LD microbiomes (Fig. 4A,B). Of these, 26 proteins overlapped between the high/low responders and LD/nLD microbiomes, 25 of which passed FDR correction (Supplemental Fig. 5, Supplemental Table 1). Specifically, prominent neutrophil-related proteins such as CRISP3 and MMP8 were upregulated among high vaccine responders, highlighting an enhanced innate mucosal immune signature, whereas LYPD3 was enriched in low responders.[32–34] Additionally, LD samples showed upregulation of proteins such as RPL8 and RPTN, whereas the nLD group was characterized by elevated levels of proteins including the antioxidant peroxiredoxin-1 (PRDX1) and CAPZB, reflecting distinct inflammatory and metabolic profiles.[35,36]

Pathway enrichment analyses revealed that proteins associated with LD microbiomes were involved in pathways related to B-cell activation, IL-12 signaling, antigen presentation via MHC, cytosolic Ca^{2+} signaling, and neutrophil degranulation (Fig. 4C). Proteins associated with high responders were involved in innate and adaptive immune processes, including IL-4 signaling, neutrophil degranulation, TGF-β signaling, IL-10 signaling, and T-cell exhaustion (Fig. 4C). Notably, several gene sets and pathways, including those related to TGF-β signaling, IL-4 signaling, neutrophil degranulation, and LPS stimulation were negatively associated with both high responders and LD participants, suggesting common inflammation and immune regulation pathways associate with both vaginal microbiome composition and vaccine-induced antibody responses (Fig. 4C).

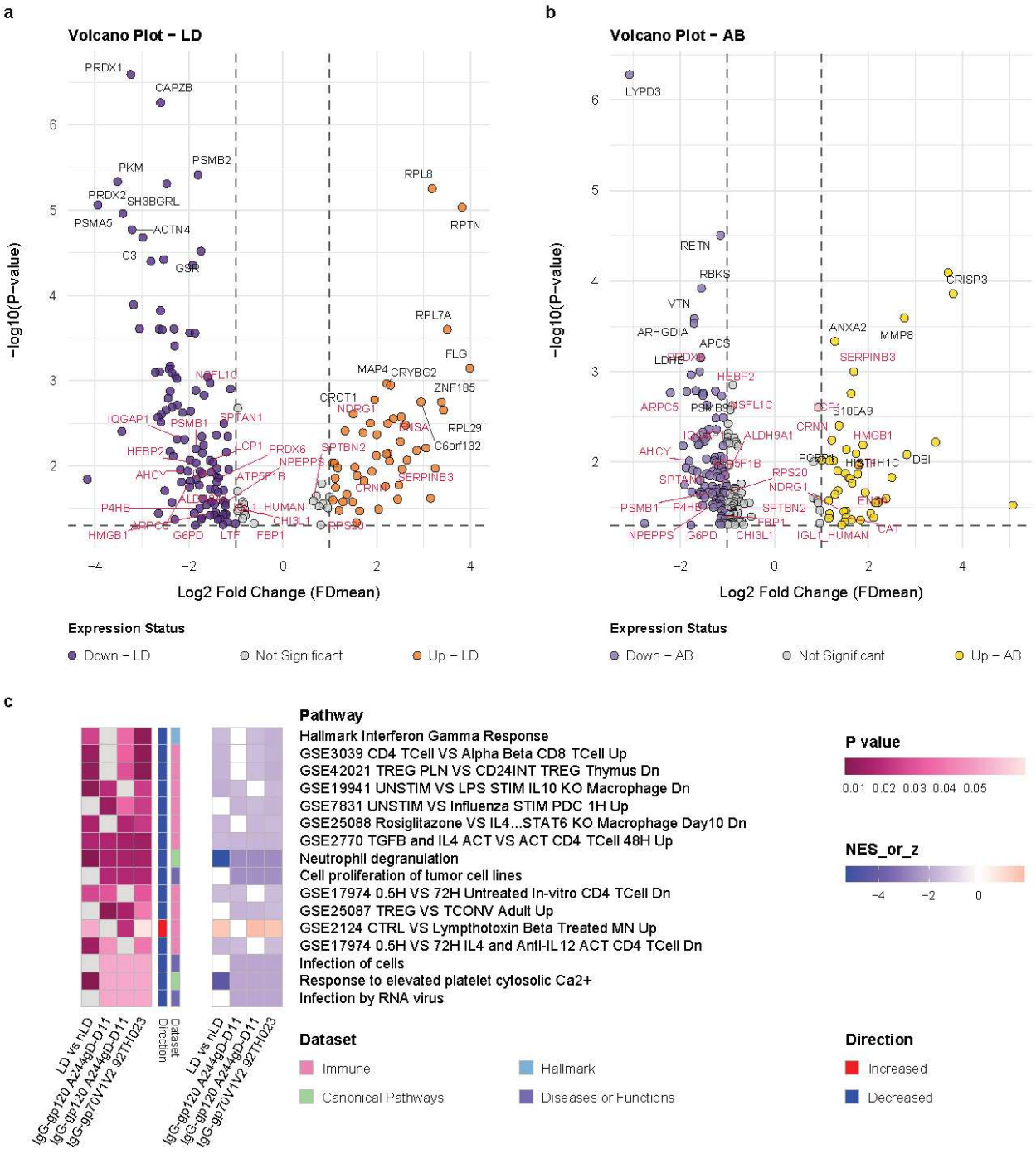


Figure 4 – Vaginal mucosal pathways associated with a higher vaccine-induced binding antibody response and LD vaginal microbiomes. Vaginal mucosal proteins and associated pathways were determined by mass spectrometry-based proteomic analysis of vaginal swab specimens. (A) Differential protein abundance for high vaccine responders compared to low vaccine responders as well as (B) LD vs. nLD individuals. (C) Pathways in

common with a higher vaccine response and LD vaginal microbiomes are shown, including the top 10 GSEA- and IPA-determined pathway differences of high responders for IgG-gp120 A244gD-D11 and IgG-gp70V1V2 92TH023, and LD vs nLD microbiomes. Pathways that were significant in at least 3 of these comparisons are shown.

PBMC Transcriptomic Profiling and LD microbiomes associated with increased systemic humoral immunity responses

Lastly, we evaluated the relationship between systemic immunity and the vaginal microbiome. Peripheral blood mononuclear cell (PBMC) transcriptomic profiling was performed using samples collected at two timepoints after completion of the RV144 vaccine regimen (3 days post- and 2 weeks post-vaccination; read counts accessible via GEO [GSE181932]), detecting expression of 16,859 genes across all participants. We then performed weighted gene co-expression network analysis (WGCNA) to identify cohorts of genes that differed in expression between LD and nLD. This approach identified 19 total modules of co-expressed genes (Fig. 5A), which ranged in size from 1473 member genes to 56 (Fig. 5B).

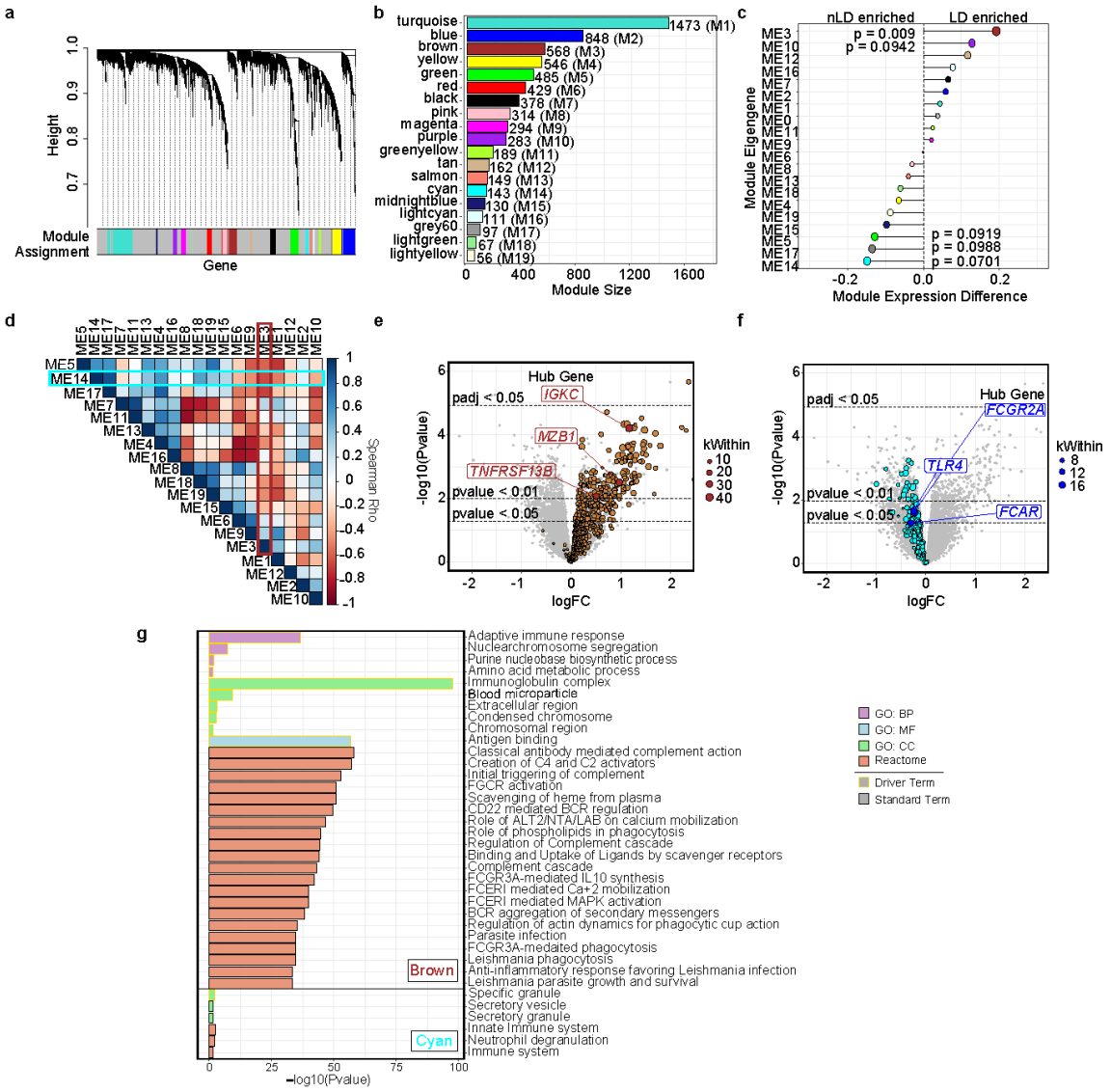


Fig 5 – Systemic transcriptomic signatures differentiating LD status. (A) Module dendrogram illustrating clusters of co-expressed genes (colored vertical bars) identified using WGCNA with PBMC transcriptomic data from RV306 at two time points after completion of the RV144 vaccination regimen (3 days and 2 weeks post final-vaccination; n = 32 samples). (B) Bar graph illustrating number of member genes assigned to each co-expression module in A (B); modules were assigned unique numeric identifiers based on ranked module size (e.g., turquoise module = M1). (C) Differences in mean module eigengenes (PC1 using each module's member genes' expression data) between samples assigned to nLD or LD microbiome status; p-values next to each point indicate if module eigengenes differ significantly ($p < 0.05$) between LD and nLD samples, as assessed using linear mixed effects models and ANOVA. (D) Heatmap depicting spearman's rho correlation coefficients between module eigengenes. Colors indicate strength of

correlation between any two given module eigengenes; two modules are depicted within colored box insets, ME3 (brown module) and ME14 (cyan module). (E,F) Volcano plot depicting differential expression analysis between LD and nLD microbiome types; x-axis indicates log2 fold-change and y-axis indicates the -log10 p-value for individual genes. Genes with positive log(FC) values are expressed at greater levels in LD samples while genes with negative log(FC) values are expressed at greater levels in nLD samples. Colored points highlight module member genes from M3 (brown; E) or M14 (cyan; F) and the size of colored points indicates intramodular connectivity (kWithin) values, a measure of centrality or hub-status for each gene. Selected hub genes with functions related to adaptive (*IGKC, MZB1, TNFRSF13B*) or innate (*FCG2RA, TLR4, FCAR*) immunity are shown in darker colors. (G) Bar graph depicting top-scoring pathways significantly enriched among M3 (brown) and M14 (cyan) member genes, identified via gProfiler overrepresentation analysis. Terms with bars highlighted in yellow are non-redundant "driver" terms for each module; terms with black outlines are standard significant hits and may be redundant to or nested within driver terms.

Module eigengene analysis revealed significant differences between LD and nLD participants for select modules, as determined by linear mixed-effects modeling and ANOVA (Fig. 5C). Correlation analysis of eigengenes from each module revealed structured relationships among co-expression modules (Fig. 5D).

The brown module (module 3) was expressed at significantly higher levels in participants with LD status and was enriched for genes involved in humoral immunity and B-cell function, including hub genes *IGKC, MZB1*, and *TNFRSF13B* (TACI) (Fig. 5E). In contrast, the cyan module (module 14) showed higher expression in nLD participants and was enriched for innate immune pathways and inflammation, including neutrophil degranulation and innate immune receptor signaling, with key genes such as *FCGR2A* (CD32a*), FCAR*, and *TLR4* (Fig. 5F). Pathway enrichment analysis (gProfiler; g:SCS-adjusted $p < 0.05$) further supported these findings, with the brown module associated with adaptive immune pathways and the cyan module enriched for innate immune signaling (Fig. 5G).

Together, these findings suggest that LD participants exhibit a systemic immune environment skewed toward adaptive, B cell–associated responses, consistent with the enhanced vaccine-induced antibody responses observed in this cohort. In contrast, nLD participants demonstrated greater expression of innate inflammatory and myeloid-associated programs, indicating a more activated basal immune state that may be less favorable for the generation of optimal humoral immunity. These transcriptomic differences support the concept that vaginal microbiome composition is associated with

distinct systemic immune phenotypes that may contribute to differences in vaccine responsiveness.

Discussion

There were two major key findings to this study. The first is that participants in the RV306 trial with *Lactobacillus*-dominant (LD) vaginal microbiomes exhibited higher mucosal and systemic HIV Env-specific binding antibody responses to the RV144 ALVAC-HIV/AIDSVAX B/E boost regimen compared to those with non-*Lactobacillus*-dominant (nLD) microbiomes. Second, LD participants showed enhanced adaptive and innate immune signatures both systemically and within the vaginal mucosa, whereas nLD participants demonstrated increased signatures of inflammation. These findings suggest that the vaginal microbiome may serve as a biomarker of immune profiles better optimized to respond to a vaccine. It is also plausible, although less likely, that the vaginal microbiome interacts with the host at both the mucosal and systemic level to promote increased innate immunity, thereby underlying a better vaccine immune response. To our knowledge, our study is the first to link vaginal microbiome composition with vaccine-induced immune responses.

The microbiome has previously been implicated in shaping vaccine immunity, both as a biomarker and as a functional contributor to immune responses. Prior studies of the gut and oral microbiome have demonstrated associations with vaccine efficacy across multiple pathogens, including typhoid, polio, and influenza.[27,37,38] In the context of HIV and other viral antigens, previous studies have identified HIV-1–reactive CD4 T cells in uninfected individuals that exhibit cross-reactivity with environmental antigens, including commensal microbial peptides.[39] These T cells were observed to recognize HIV-1, CMV, and HSV epitopes based on cross-reactivity with microbial peptides from *Ruminococcus*, *Lachnospiraceae*, and *Bifidobacterium*, supporting prior antigenic priming.[39] Influenza-reactive CD4 T cells also cross-reacted with peptides from *Finegoldia magna*.[39] Also observed was the recognition of HIV-1 peptides by naive and memory CD4 T in seronegative individuals, with microbial sequence homology suggesting environmental priming.[40] Together, these findings support microbial antigen–driven pre-priming of antiviral CD4 T cell repertoires that may influence vaccine responses.

Additionally, microbiota have been shown to shape vaccine responses across diverse vaccine platforms through modulation of innate immune signaling and downstream adaptive immune priming. In adults, antibiotic-induced disruption of the microbiome and loss of flagellated taxa have been associated with reduced influenza vaccine antibody responses, linked to impaired TLR5–NF-κB signaling and diminished dendritic cell

activation.[41] In contrast, enrichment of commensal-derived microbial metabolites such as short-chain fatty acids (SCFAs) has been linked to enhanced T follicular helper (Tfh) cell differentiation and improved humoral responses in infant vaccination cohorts, including BCG, polio, and pneumococcal vaccines.[42] The success of oral rotavirus vaccines have similarly been associated with microbiome states enriched in *Bifidobacterium* species, which was linked to enhanced mucosal IgA responses and increased seroconversion.[43] In adults, gut dysbiosis characterized by reduced SCFA-producing taxa such as *Faecalibacterium* has been associated with diminished responses to SARS-CoV-2 vaccination, further supporting a role for microbiome-driven immune tone in shaping systemic vaccine immunogenicity.[44]

Accumulating evidence indicates that microbiota also influence viral immunity through systemic, distal immune effects. Interferon-β responses in the lungs were linked to acetate production from intestinal microbiota and were shown to mediate viral load of RSV.[45] Furthermore, antibiotic depletion of the gut microbiota was seen to reduce baseline interferon-stimulated gene expression in pleural epithelium cells, resulting in an impaired early antiviral state and diminished downstream immune responses to viral infection.[46] In the context of vaccination, rhesus macaques receiving an HIV vaccine regimen demonstrated a correlation between rectal microbiome composition and vaccine-induced humoral responses, with *Lactobacillus*- and *Clostridia*-enriched communities associated with higher gp120/gp140 antibody responses, while *Prevotella*-enriched profiles were associated with weaker responses.[47] Our findings translate and extend these cross-species observations to a clinical cohort, providing the first human evidence that a *Lactobacillus*-dominant mucosal environment corresponds with significantly heightened HIV-specific IgG responses both systemically and at the vaginal mucosa. By demonstrating that human *Lactobacillus* dominance mirrors the antibody-boosting phenotypes observed in non-human primates, these data reinforce a conserved, cross-species role for *Lactobacillus* taxa in optimizing vaccine-induced humoral immunity.

Importantly, the microbiome can also be dynamically influenced by vaccination itself, suggesting the possibility of bidirectional interactions between host immune activation and microbial community structure. Intranasal live attenuated influenza vaccination has been shown to induce measurable shifts in the upper respiratory tract microbiome, including changes in community composition and relative abundance of dominant bacterial genera within weeks following immunization.[48] Intramuscular administration of inactivated and mRNA SARS-CoV-2 vaccines has been associated with reduced bacterial diversity and compositional shifts in the intestinal microbiota one month after vaccination.[49] However, other studies, including those examining the vaginal microbiome, have observed no microbiome compositional shifts post-vaccination, suggesting that vaccine-associated

microbial changes may vary depending on the mucosal site, vaccine platform, and local immune environment.[50,51]

Although direct evidence linking the vaginal microbiome to vaccine immunogenicity in humans remains limited, substantial evidence demonstrates that vaginal microbial composition strongly shapes local immune activation and mucosal barrier function. *Lactobacillus*-dominant (LD) vaginal microbiomes are associated with lower inflammation, improved epithelial barrier integrity, and reduced HIV acquisition risk, whereas non-Lactobacillus-dominant (nLD) communities and bacterial vaginosis are associated with increased inflammatory cytokines, immune cell recruitment, epithelial disruption, and heightened susceptibility to HIV infection.[11,19] While vaccination itself can also alter host–microbiome interactions, within our cohort LD and nLD states remained relatively stable over time, suggesting that baseline microbial composition may contribute more strongly to vaccine responsiveness than vaccination-induced microbiome shifts. In our study, LD participants exhibited enhanced mucosal and systemic antibody responses together with proteomic signatures consistent with coordinated innate and adaptive immune activation, including enrichment of IL-4 signaling, TGF-β signaling, and antigen presentation. In contrast, nLD participants demonstrated heightened inflammatory and innate immune signatures characterized by neutrophil activation and increased monocyte/macrophage-associated responses.

Systemic transcriptional profiling reinforced these observations. Network analysis of PBMC transcriptomes identified a B cell–associated gene module enriched in LD participants, characterized by member genes involved in humoral immunity, including *IGKC*, *MZB1*, and *TNFRSF13B*. In contrast, nLD participants exhibited enrichment of an innate immune–associated module driven by genes involved in neutrophil activation and Fc receptor signaling. These opposing transcriptional programs suggest that vaginal microbiome composition is linked not only to local mucosal conditions but also to systemic immune polarization, with LD states favoring coordinated antibody responses and nLD states associated with heightened innate immune activation.

The distinct mucosal proteomic and systemic transcriptomic profiles observed in our cohort underscore a fundamental divergence in how local microbial environments shape the innate-to-adaptive immune conduit required for effective vaccination. In LD individuals, mucosal enrichment of IL-4 and TGF-β signaling pathways provides a critical homeostatic microenvironment that favors balanced antigen presentation and downstream humoral activation.[12,52] This local baseline likely primes the systemic compartment, driving the expansion of the B-cell-associated transcriptional module we identified. Within this module, we observed a marked upregulation of *IGKC*, which likely

indicates a robust, active B-cell response and the generation of plasma cells capable of producing antibodies.[53] Additionally, upregulation of *MZB1*, a critical chaperone for IgM and IgG secretion, and *TNFRSF13B*, which mediates plasma cell differentiation, points to an immune tone optimized for robust antibody production.[54,55] Conversely, nLD-associated mucosal and systemic profiles were characterized by chronic, hyper-inflammatory innate activation, featuring overt neutrophil degranulation and upregulated signaling axes like *FCGR2A*, *TLR4,* and *FCAR*, which perpetuate a state of immunological exhaustion and localized tissue stress.[56] While acute innate signaling, such as the TLR5–NF-κB axis previously observed in successful viral and influenza vaccinations is indispensable for downstream adaptive priming, chronic mucosal dysbiosis and sustained TLR4-driven inflammation in nLD states appear to decouple this relationship.[27] Instead of promoting protective humoral immunity, this persistent innate activation polarizes the systemic immune tone away from coordinated B-cell maturation, ultimately resulting in the diminished vaccine-induced antibody responses observed in our nLD cohort.

There are several limitations to this study that should be considered. First, the sample size for the primary comparison was modest and unbalanced (consistent LD n = 43; consistent nLD n = 18), which limited statistical power to detect anything beyond large effect sizes (estimated power to detect moderate effects [$d \approx 0.5$] = 58% at $\alpha = 0.05$). Furthermore, the discretization of continuous antibody titers into ordinal response groups further reduced sensitivity to detect smaller magnitude effects. Together, these factors suggest that while robust associations may be reliably detected, more modest effect sizes may not have been adequately powered in the present analysis. Additionally, although we identified significant associations across multiple analyses, the observational design precludes causal inference, and it remains unclear whether microbiome composition directly influences vaccine responses or instead reflects underlying host or environmental factors. Finally, the study population was limited to women in Thailand, which may affect the generalizability of these findings to other populations with different genetic backgrounds, environmental exposures, and baseline microbiome compositions.

Overall, our findings indicate that vaginal microbiome composition is associated with differences in vaccine-induced antibody responses and systemic immune profiles in the context of HIV vaccination. This suggests that the vaginal microbiome may represent a biomarker of increased innate immunity and vaccine immune responses. Future studies should investigate the mechanistic basis of these associations and explore whether targeted interventions to promote *Lactobacillus* dominance can improve immune outcomes for HIV and other mucosal vaccines.

Methods

Author Contributions

A.D.B, A.S., R.P., R.T. and C.H. conceived the microbiome sub-study. A.Y., O.C., M.C., F.C.M., M.P., O.T., S.A., S.B., performed the experimental analysis of swab specimens and generated the mass spectrometry and metagenomics data. L.R.M, A.B., M.H., L.N.R, S.K. performed data cleaning and analyses and L.R.M, A.B., M.H., L.N.R, S.K., A.S., R.P., R.T, and A.D.B interpreted the data. S.R, S.A., S.N.S.C, P.P., S.R, J.A.A, S.V., and A.S managed the study cohort and clinical trial. L.R.M, A.B., M.H., R.T., A.S., and A.D.B wrote the paper. All authors contributed to the review and editing of the paper.

Acknowledgments

We would like to thank all RV306 participants for making this study possible. This project was supported by a Canadian Institutes of Health Research Innovative Biomedical and Clinical HIV/AIDS Research Team Grant, project number: HB3-164066. Dr. Burgener receives support from the National Institutes of Health, including award number R01CA266050, the Rustbelt Center for AIDS Research (2P30AI036219-26A) and the CWRU Center for Excellence on Substance Use and HIV (5P30DA054557). Dr. Burgener also receives funding support from the European Union's Horizon 2020 research and innovation program under grant agreement No. 847943 (The Mistral project). The funders had no role in study design, data collection and analysis, decision to publish or preparation of the manuscript.

Competing Interests

The authors declare no competing interests.

Funding

Funding was received via Innovative Biomedical and Clinical HIV/AIDS Research Team Grant, project number: HB3-164066.

Disclaimer

Material has been reviewed by the Walter Reed Army Institute of Research. There is no objection to its presentation and/or publication. The opinions or assertions contained herein are the private views of the author, and are not to be construed as official, or as reflecting true views of the Department of the Army or the Department of War.

STAR★METHODS

KEY RESOURCES TABLE

REAGENT or RESOURCE	SOURCE	IDENTIFIER
Biological Samples		
Cervicovaginal mucus (CVM) and blood samples (n = 97)	RV306 Clinical Trial (Thailand sites)	ClinicalTrials.gov: NCT01931358
Chemicals, Peptides, and Recombinant Proteins		
Dithiothreitol (DTT)	Sigma Aldrich Fine Chemicals Biosciences DLDITHIOTHREITOL, >=98% (HPLC)	Cat# 50-184-5440
Iodoacetamide (IAA)	Supply Solutions Sigma; Iodoacetamide Bioultra-25G in glass bottle * Third Party Item	Cat# NC0978506
Urea	GE Healthcare PlusOne™ Reagents	Cat# 45-000-234
Benzonase Endonuclease	Thermo Scientific™ Pierce™ Universal Nuclease for Cell Lysis	Cat# 88700
Sequencing Grade Modified Trypsin	Thermo Scientific™ Mass Spectrometry Grade Proteases	Cat# A40009
Ammonium Formate	Thermo Scientific Chemicals Ammonium formate, 98+%	Cat# 540-69-2
Acetonitrile (LC-MS Grade)	Thermo Fisher Scientific Acetonitrile (HPLC), Fisher Chemical- Case of 4	Cat# A998-4
Formic Acid (LC-MS Grade)	Thermo Fisher Scientific Formic acid, Puriss. p.a., ACS Reagent, Reag. Ph. Eur., ≥98%, Honeywell Fluka™	Cat# 60-006-10
Critical Commercial Assays		
PureLink Microbiome DNA Purification Kit	Invitrogen	Cat# A29790
Qubit dsDNA HS Assay Kit	Life Technologies	Cat# Q32851
Nextera XT DNA Library Preparation Kit	Illumina	Cat# FC-131-1024
Novagen BCA Protein Assay Kit	EMD Millipore	Cat# 71285
Nanosep 10K Centrifugal Devices	Pall Corporation	Cat# OD010C33

Pierce Quantitative Fluorometric Peptide Assay	Thermo Fisher Scientific	Cat# 23290
PAXgene Blood RNA Kit	Qiagen	Cat# 762164
GLOBINclear Human Kit	Thermo Fisher Scientific	Cat# AM1980
SMART-Seq v4 Ultra Low Input RNA Kit for Sequencing	Takara Bio	Cat# 634888
MiSeq Reagent Nano Kit v2 (300-cycles)	Illumina	Cat# MS-103-1001
NovaSeq 6000 S2 Reagent Kit (300 cycles)	Illumina	Cat# 20012862
Deposited Data		
Bulk RNA-Seq Raw and Processed Read Counts	GEO	GEO: GSE181932
Shotgun Metagenomic Raw Reads	PRIDE	PXD082593
CVM Mass Spectrometry Proteomics Raw Data	PRIDE	PXD082593
Human Genome Reference (GRCh38 / hg38)	NCBI / Ensembl	GRCh38.p13
VIRGO Vaginal Non-Redundant Gene Catalog	VIRGO	VIRGO Database
UniProtKB/Swiss-Prot Human Proteome	UniProt	UniProt Consortium
Experimental Models: Organisms/Strains		
Human: Healthy HIV-uninfected female cohort (n = 97)	RV306 Clinical Trial	N/A
Software and Algorithms		
FastQC (v0.11.x)	Babraham Bioinformatics	RRID: SCR_014583
Trimmomatic (v0.33 & v0.36+)	Bolger et al., 2014	RRID: SCR_011848
Bowtie2 (v2.x)	Langmead and Salzberg, 2012	RRID: SCR_016368
MaxQuant (v1.6.5)	Cox and Mann, 2008	RRID: SCR_014485
Perseus (v2.0.3.0)	Tyanova et al., 2016	RRID: SCR_015753
Mascot Daemon (v2.4.0)	Matrix Science	RRID: SCR_000592
Scaffold (v4.8.3)	Proteome Software	RRID: SCR_014345
Fastp (v0.19.7)	Chen et al., 2018	RRID: SCR_016962
HISAT2 (v2.1.0)	Kim et al., 2019	RRID: SCR_015530
STAR (v2.4.2a)	Dobin et al., 2013	RRID: SCR_004669

HTSeq (v0.6.1–0.9.1)	Anders et al., 2015	RRID: SCR_011867
R (v4.5.2)	R Foundation for Statistical Computing	RRID: SCR_001905
edgeR (v4.8.2)	Robinson et al., 2010	RRID: SCR_012802
WGCNA (v1.7x)	Langfelder and Horvath, 2008	RRID: SCR_003302
gprofiler2	Kolberg et al., 2020	RRID: SCR_018190
Ingenuity Pathway Analysis (IPA)	QIAGEN Digital Insights	RRID: SCR_008653
GSEA	Subramanian et al., 2005	RRID: SCR_003199
Other		
Instant Softcup	Instead Healthcare	N/A
Illumina HiSeq X Ten	Illumina	RRID: SCR_016385
Agilent 1260 Infinity II HPLC System	Agilent Technologies	RRID: SCR_019355
EASY-nLC 1000 System	Thermo Fisher Scientific	Cat# LC120
Q Exactive Plus Hybrid Quadrupole-Orbitrap	Thermo Fisher Scientific	RRID: SCR_018706
Easy-Spray C18 Column (ES803; 50 cm x 100 µm, 1.8 µm)	Thermo Fisher Scientific	Cat# ES803
Illumina NovaSeq 6000	Illumina	RRID: SCR_016387

RESOURCE AVAILABILITY

Lead Contact

Further information and requests for resources and reagents should be directed to and will be fulfilled by the lead contact, Adam D. Burgener (adam.burgener@case.edu).

Materials Availability

This study did not generate new unique reagents.

Data Availability

Data: Bulk RNA sequencing read counts have been deposited at GEO under accession number GEO: GSE181932 and are publicly available. Raw shotgun metagenomics and mass spectrometry proteomics files have been deposited on PRIDE. Data are available via ProteomeXchange with identifier PXD082593. Accession numbers are listed in the Key Resources Table.

Any additional information required to reanalyze the data reported in this paper is available from the lead contact upon reasonable request.

EXPERIMENTAL MODEL AND SUBJECT DETAILS

Human Ethics Approval

Ethical approval was obtained from institutional review boards (CWRU IRB# [20200059]). Written informed consent was obtained from all participants prior to study inclusion.

Human Cohort and Clinical Design (RV306)

The RV306 clinical trial (ClinicalTrials.gov NCT01931358: 2013-08-12) was conducted in healthy Thai volunteers as previously described (Pitisuttithum P, et al. Late boosting of the RV144 regimen with AIDSVAX B/E and ALVAC-HIV in HIV-uninfected Thai volunteers:

a double-blind, randomised controlled trial. Lancet HIV. 2020;7(4):e238–e248). For the current study healthy, HIV-uninfected female participants (20–40 years of age; n = 97) were enrolled across three clinical sites in Thailand: (1) Vaccine Trial Centre, Mahidol University (Bangkok); (2) Royal Thai Army Clinical Research Center, AFRIMS (Bangkok); and (3) Research Institute for Health Sciences, Chiang Mai University (Chiang Mai).

All participants previously completed the primary RV144 vaccination series and were randomized to receive the RV306 late-boost regimen (n = 88) or placebo (n = 9). Late boosts (ALVAC-HIV and/or AIDSVAX B/E at 12, 15, or 18 months) were administered outside the sampling window of the present analysis.

Longitudinal collection of cervicovaginal mucus (CVM) and peripheral blood occurred at three primary visits: (1) Baseline (V0; Week 0): Pre-vaccination, (2) Visit 4 (V4; Week 14): 2 weeks post-first boost, (3) Visit 6 (V6; Week 26): 2 weeks post-second boost.

METHOD DETAILS

Sample Collection and Processing

Peripheral Blood: Whole blood was processed for peripheral blood mononuclear cell (PBMC) isolation using standard Ficoll density-gradient centrifugation. Isolated PBMCs were cryopreserved at −80°C for downstream RNA extraction. Plasma was collected following whole blood clotting and centrifugation, and stored at −80°C for systemic HIV-specific antibody quantification.

Cervicovaginal Mucus (CVM): Single CVM samples were collected by Instant SoftcupTM during pelvic examinations and immediately stored at −80°C. Aliquots were prepared for

microbiome profiling, metabolomics, host proteomics, and bacterial proteomics processing.

Shotgun Metagenomic DNA Extraction and Sequencing

Total microbial DNA for shotgun metagenomic sequencing was extracted and purified from each vaginal CVM sample using the Purelink Microbiome DNA Purification Kit (Invitrogen, U.S.) according to the manufacturer's instructions. DNA concentrations were measured using the Qubit dsDNA HS Assay kit (Life Technology, U.S.). Extracted DNA was fragmented using the Nextera-XT DNA Library Kit (Illumina, U.S.) and one library of 300-bp average clone insert size was constructed for each sample. All sequencing libraries were pooled and processed on an Illumina HiSeqX10 platform (Illumina, U.S.) by Macrogen Genomic Division Korea.

CVM Mass Spectrometry Sample Preparation and Fractionation

For proteomic analysis, CVM samples were processed using a standardized pipeline,[57] with modifications tailored to this study. Protein content of CVM samples was quantified using the Novagen BCA Protein Assay Kit. Samples were then concentrated using Nanosep 10K filtration cartridges and denatured in urea exchange buffer (8 M urea, 50 mM HEPES, pH 8.0). Proteins were reduced with dithiothreitol (DTT, 25 mM) and alkylated with iodoacetamide (IAA, 9.26 mg/mL) to disrupt disulfide bonds and protect cysteine residues. To minimize nucleic acid contamination, samples were treated with Benzonase prior to digestion. Proteins were subsequently digested overnight at 37°C with trypsin (2 µg per 100 µg protein) within the filtration cartridge.

Peptides were recovered by sequential elution with HEPES buffer, pooled, and dried by vacuum centrifugation prior to storage at −80°C. Peptide concentrations were determined using the Pierce Quantitative Fluorometric Peptide Assay, and samples were normalized to a final concentration of 0.125 µg/µL in nanoLC Buffer A (2% acetonitrile, 0.1% formic acid). For quality control and batch alignment, a master mix was generated by pooling aliquots from all samples and analyzed periodically throughout LC-MS/MS runs.

Peptide cleanup and fractionation were performed using high-pH reversed-phase liquid chromatography on an Agilent 1260 Infinity II HPLC system equipped with a Waters 4.6 × 50 mm column. Peptides were resuspended in HPLC Buffer A (20 mM ammonium formate, pH 10) and separated using a gradient of aqueous (Buffer A) and organic (Buffer B: 90% acetonitrile, 20 mM ammonium formate, pH 10) solvents to remove salts and other contaminants. The column was equilibrated by incrementally increasing flow rates from 0.1 to 1.0 mL/min prior to peptide elution. Peptides were eluted under increasing organic

conditions, collected as fractions, dried by vacuum centrifugation, and resuspended in nanoLC Buffer A prior to mass spectrometry analysis.

LC-MS/MS Data Acquisition

Peptides from each sample (~1 µg) were analyzed using a nano-flow Easy-nLC 1000 system coupled in-line to a Q Exactive Plus mass spectrometer equipped with a nano-electrospray ion source operated at 2.0 kV (Thermo Fisher Scientific, Waltham, MA). Peptides were loaded onto a C18 reversed-phase Easy-Spray column (ES803; 50 cm length, 100 µm inner diameter, 1.8 µm particle size) and separated using a linear gradient of increasing organic solvent (2–30% acetonitrile with 0.1% formic acid) over ~120 minutes at a flow rate of ~200 nL/min.

Full MS survey scans were acquired in the Orbitrap mass analyzer over an m/z range of 300–1700 at a resolution of 70,000 (at m/z 200), with an automatic gain control (AGC) target of 3×10^6 and a maximum injection time of 80 ms. Data-dependent acquisition was employed, selecting the most abundant precursor ions for fragmentation by higher-energy collisional dissociation (HCD; 28% normalized collision energy), with precursor selection criteria including an isolation width of 3 m/z, intensity threshold of 1×10^5 ions, and charge states of +2 to +5. MS2 spectra were acquired in the Orbitrap at a resolution of 17,500 (at m/z 200), with an AGC target of 2×10^5 and a maximum injection time of 100 ms. Dynamic exclusion was applied to minimize repeated sampling of abundant ions.

Reference and quality control samples consisting of pooled CVM material were included throughout runs (approximately every 10 injections) to monitor instrument performance and enable downstream normalization. Sample quality was assessed based on total protein signal intensity within each batch. Samples with median protein abundance exceeding 1.5 times the interquartile range were considered outliers and excluded from downstream analysis.

PBMC Bulk RNA Sequencing

RNA was extracted from whole blood collected at two timepoints as part of the RV306 (3 days post final vaccination and two weeks post final vaccination, n = 32 total) using the PAXgene and GlobinClear purification kits (Qiagen, Germantown, MD; ThermoFisher Scientific, Waltham MA) following manufacturer's specifications. Synthesis of cDNA was carried out using 10 ng of RNA input with the SMART-Seq V4 UltraLow RNA Prep Kit (Takara Bio, Inc.) and control RNA spike-in (ThermoFisher Scientific) and subsequent libraries were prepared using the Nextera XT DNA Sample Prep Kit (Illumina, San Diego, CA). Libraries were sequenced twice; once to quantify individual sample concentration in library pools via Illumina MiSeq (PE; 300 cycles; Nano Kit v2) and then using adjusted library pools via

Illumina NovaSeq 6000 (PE; 300 cycles; S2 XP). Resulting reads from the NovaSeq run were demultiplexed and quality filtered with Fastp (v0.19.7) and Trimmomatic (v0.33) using default parameters.[58]

QUANTIFICATION AND STATISTICAL ANALYSIS

Metagenomic Data Processing and VIRGO Classification

Quality assessment of raw sequencing data was performed using the FastQC software.[59] Total sequences were filtered by length and quality using Trimmomatic[60] (minimum base quality for both leading and trailing bases = Q30; minimum basepairs length = 75; minimum quality average for 30-bp sliding windows across sequences = Q20). Human DNA contamination was removed by aligning filtered paired-end reads against the human genome (hg38) using Bowtie2.[61] Reads uniquely aligned to the human reference with quality score higher than Q20 were discarded. Taxonomy classification and microbial species composition were determined using the human vaginal non-redundant gene catalog (VIRGO).[62]

Proteomic Data Processing (Host and Bacterial)

Host Proteomics: Raw reads from MS were processed via MaxQuant (v 1.6.5) and Perseus (v2.0.3.0) before performing quality control (QC) and cleaning in R. The UniProt/Swissprot database was used for alignment to reads during MaxQuant. A total of 1797 total human proteins were detected by MS (<25% CoV on Log2 NA data), but only 754 were consistently identified in every batch and therefore used in analysis. Batches were adjusted for batch effects using an empirical Bayes formula.

Bacterial Proteomics: Raw spectra were aligned and filtered, and peptides were identified using Mascot Daemon (v2.4.0) against the SwissProt/UniProtKB human database.[63] Scaffold software (v4.8.3)[64] confirmed protein identifications with ≤1% FDR at the protein level, ≤0.1% FDR at the peptide level, and ≥2 unique peptides. Host proteome data were log2-transformed and batch-corrected using ComBat.[65]

Microbiome Stratification (LD/nLD and CST)

Participants were classified based on vaginal microbiome composition derived from metaproteomic analyses of cervicovaginal mucus (CVM) samples. Lactobacillus dominance (LD) versus non-dominance (nLD) was determined by the relative abundance of total Lactobacillus proteins in each sample: participants with ≥50% of total Lactobacillus content were classified as LD, and those with <50% as nLD. Community State Types (CSTs) were similarly defined based on dominant Lactobacillus species, with participants categorized as *L. crispatus*–dominant, *L. iners*–dominant, or polymicrobial.

Metagenomic sequencing data were used as a secondary validation to assess concordance with metaproteomic-based classification. Metaproteomic microbiome classifications were used for all downstream analyses, including diversity analyses, antibody comparisons, and transcriptomic analyses.

Diversity, Quantification, and Antibody Comparisons

Alpha/Beta Diversity: Alpha diversity was calculated using the Shannon H index and visualized in R (packages: dplyr, plyr, tidyr, vegan, ggplot2, ggpubr). Longitudinal alpha diversity was also assessed across all three timepoints. P-values were calculated and visualized using the *stat_compare_means* function in ggpubr.

Beta diversity was assessed using Bray-Curtis distances and visualized via Principal Coordinates Analysis (PCoA) in R (packages: vegan, ggplot2). Longitudinal beta diversity was examined for both LD status and CST groups across all three timepoints.

Antibody Quantification: HIV-specific antibody responses were quantified by enzyme-linked immunosorbent assay (ELISA) using plasma and CVM samples. Antibody responses associated with vaccine immunogenicity were identified by t-test and three significant relationships were identified: mucosal IgG binding to gp120 A244, mucosal IgG binding to gp70 V1V2 92TH023, and plasma IgG binding to gp120 A244.

Categorical assignments of response level for these three antibodies were determined through tertiles, with non-responders being at the minimum threshold for detection, low responders below the middle tertile, medium responders from the middle to upper tertile, and high responders being the upper tertile. Due to small group sizes, low responders were combined with non-responders for downstream analyses. In depth IgG-gp120 A244 in mucosa had high responder >= 51200, medium < 51200 and > 12800, and low responders <= 12800. For IgG-gp70V1V2 92TH023, high responders were >= 6400, medium < 6400 and > 1600, and low <= 1600. For IgG-gp120 A244 in plasma, high >= 800, medium < 800 and > 150, and low <= 150.

Antibody Comparisons: Analyses were restricted to participants with consistent microbiomes across all three timepoints (n = 61; longitudinal microbiome changes = LD→LD→LD or nLD→nLD→nLD). Comparisons were made between LD vs nLD and among CST groups. Both metaproteomic and metagenomic datasets were analyzed: metaproteomic classifications were used for primary stratification, while metagenomic data were used to validate classification concordance.

Broadly, proportional data was used for all microbiome analyses (Fig. 1 and 2). For longitudinal analyses, all results were based on paired data from patients' follow-up

683 samples. Microbiome data was used to compare LD/nLD status, along with alpha and beta
684 diversity (Fig. 1 and 2). Levels of *Lactobacillus* were compared to other *Lactobacillus*
685 species versus all other taxa for LD classification. Those ≥50% *Lactobacillus* species were
686 classified as LD, all others were classified as nLD. PERMANOVA p-values are listed on the
687 beta diversity figures for each analysis, with significance seen as ≤ 0.05.

688 Comparisons of antibody level in both plasma and mucosa were made between
689 microbiome (LD vs nLD) categories using two-sample unpaired t-tests on raw antibody
690 levels measured at the final visit (V6, week 26; Fig. 3). Two-sample unpaired t-tests were
691 also used to compare antibody levels among CST groups, with each CST group compared
692 individually against the other two. Only tests consistent with the alternative hypothesis of
693 higher antibody levels were considered. T-tests were performed in R using the *t.test*()
694 function with default parameters, except when longitudinal data was investigated, then a
695 paired *t.test(paired = TRUE)* was performed. P-values of associated analyses are displayed
696 within figures, with a value of ≤ 0.05 deemed significant.

697 **RNA-Seq Processing and Differential Gene Expression**

698 Quality-trimmed reads were aligned to the human genome (GRCh38.p13; build 88-92) via
699 Hisat2 (v2.1.0) or STAR (v2.4.2a) and resulting alignments were counted to generate read
700 counts via HTSeq (v0.6.1-0.9.1).[66–68]

701 Differences in gene expression between were assessed by fitting read counts to a quasi-
702 likelihood negative binomial generalized log-linear model as implemented using edgeR
703 (v4.8.2) in R (v4.5.2), with low-expression genes filtered using *filterByExpr*, followed by
704 quasi-likelihood negative binomial modeling (*glmQLFit*) and quasi-likelihood F-tests
705 (*glmQLFTest*). Differentially expressed genes (DEGs) were classified at an unadjusted p-
706 value threshold <0.01.

707 **Weighted Gene Co-expression Network Analysis (WGCNA)**

708 Weighted gene co-expression network analysis (WGCNA) was employed to identify
709 clusters (modules) of co-expressed genes associated with different microbiome types.[69,70]
710 Log-transformed counts per million (cpm) values were used to construct a single signed
711 co-expression network using the WGCNA function *blockwiseModules* with the following
712 parameters: corType = “bicor”, networkType = “signed”, TOMType = “signed”, pamStage = F,
713 maxBlockSize = 16859, minModuleSize = 50, deepSplit = 2, mergeCutHeight = 0.1,
714 maxPOutliers = 0.1, and power = 11.

715 The soft-thresholding power was selected from a range of 1–20 as the lowest value that
716 achieved a scale-free topology model fit (SFT.R^2 ≥ 0.8) while maintaining mean connectivity
717 (k) ≤ 100.

Module eigengenes (ME), defined as the first principal component of gene expression values within each module, were used as summary expression profiles for each module and screened for differences between microbiome types using linear mixed-effects models (nlme package function *lme*; ME ~ microbiome type * Visit, random = ~1|PID; one model per module). Residual normality and homoscedasticity were assessed using the Shapiro–Wilk test, Levene's test, and visual inspection of residual plots; variables were transformed as necessary to meet model assumptions. Statistical significance of microbiome-associated differences in eigengene expression was assessed using ANOVA on fitted models.

Associations between module eigengenes were evaluated with pairwise Spearman correlations (psych package function: *corTest*) and resulting correlation coefficients were visualized using the corrplot package. Intramodular connectivity (kWithin) was calculated using the WGCNA function *intramodularConnectivity* with the following parameters: corFnc = "bicor", distFnc = "dist", method = "euclidean", networkType = "signed", and power = 11. Genes with high kWithin values were considered highly connected, with the top-ranked gene in each module defined as the hub gene.

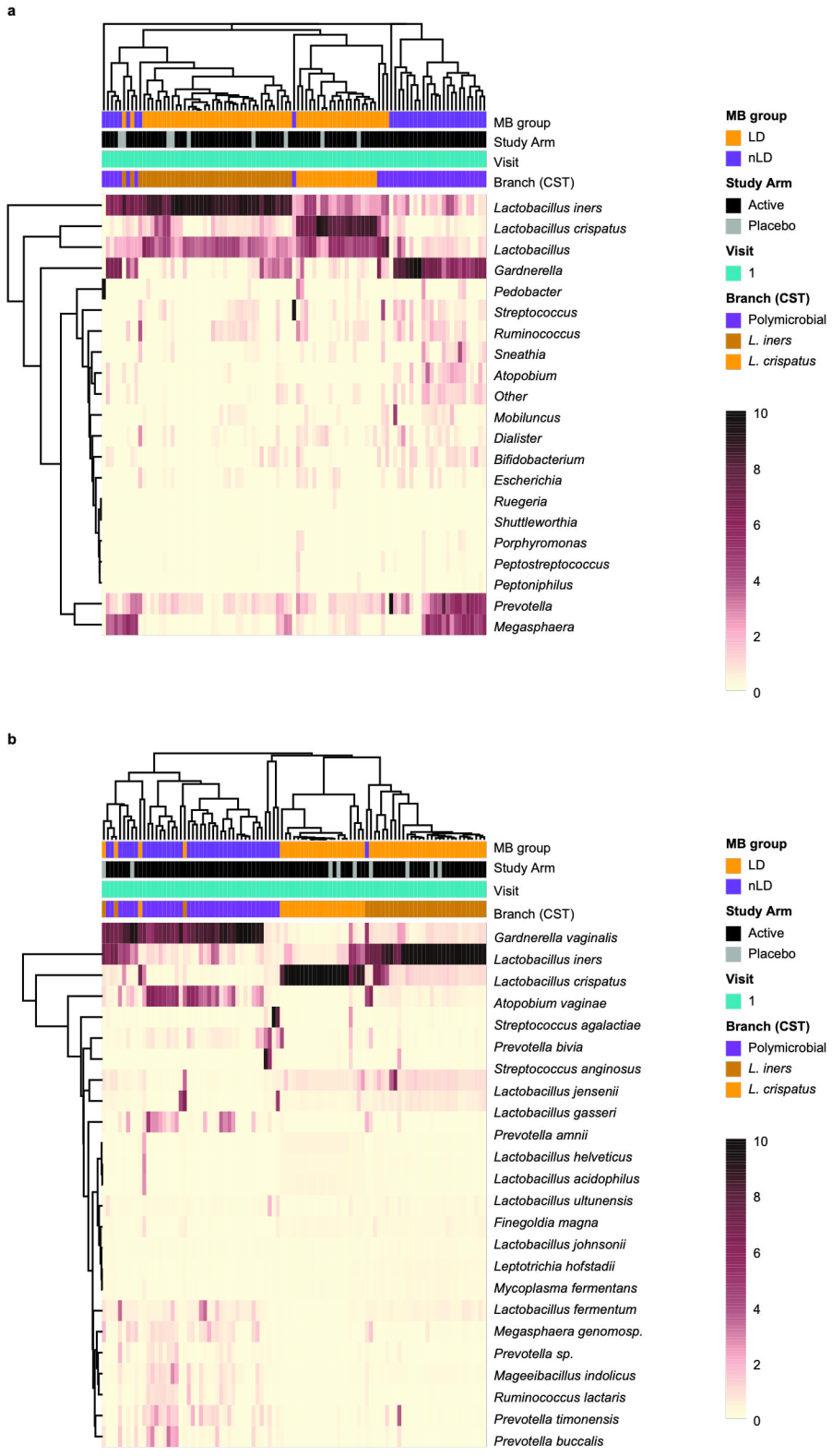
Pathway Enrichment Analysis

Log2 fold-change values for protein abundances were calculated for both LD vs nLD participants and high vs low antibody responders (Fig. 4, Supplemental Table 2). These log2 fold-change values were used as input for Gene Set Enrichment Analysis (GSEA) and Ingenuity Pathway Analysis (IPA) to identify enriched host pathways. Only pathways that were significant in at least three of the four comparisons (LD vs nLD and high vs low for each antibody) were carried forward for further interpretation.

Gene Ontology (GO) and pathway enrichment for DEGs and WGCNA modules were performed using overrepresentation analysis implemented in the R package gprofiler2 function *gost*. Differentially expressed genes (DEGs) associated with specific microbiome types, as well as genes within selected WGCNA modules, were tested for enrichment against a background of all 16,859 genes passing low-expression filtering and possessing valid annotations. Multiple testing correction and term redundancy reduction were applied using the gProfiler "g:SCS" algorithm and "highlighting" approach, respectively, to identify key driver pathways while minimizing redundant parent–child GO term reporting.

Supplemental Figures

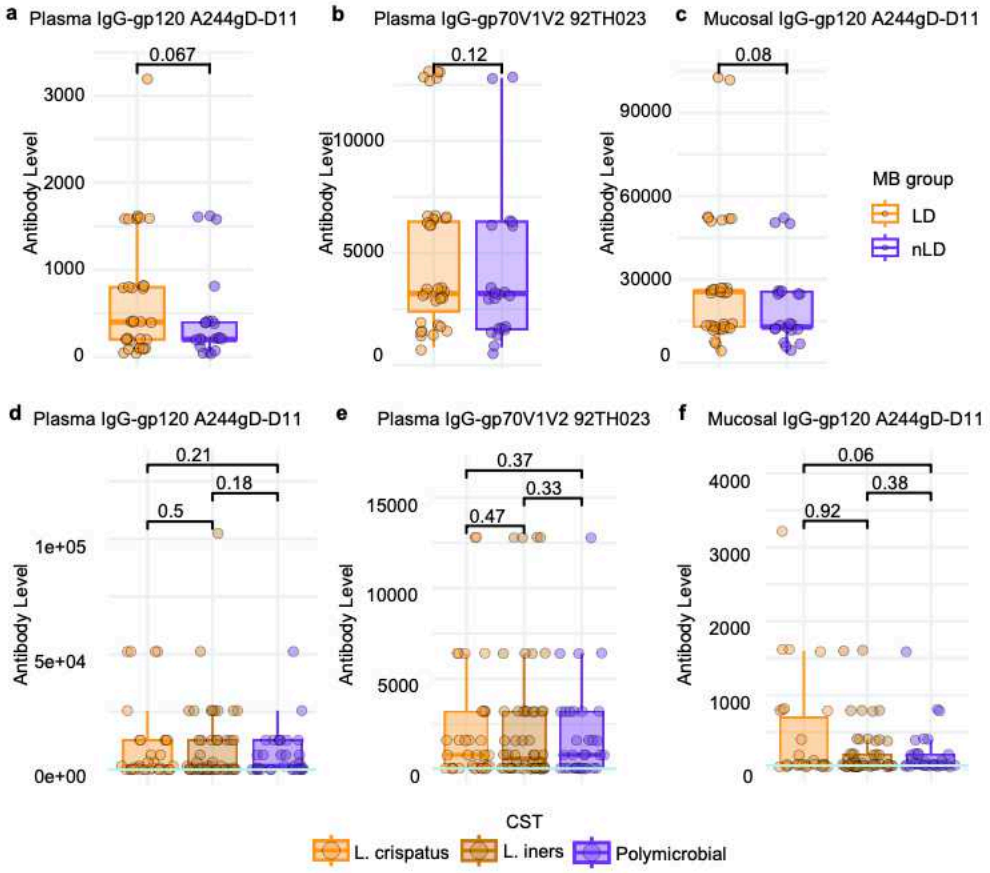
Supplemental Figure 1



Participant Vaginal Microbiota Characterization. Heatmap of microbiome composition as shown by (A) metaproteomics and (B) metagenomics for all subjects at initial visit. Bray-

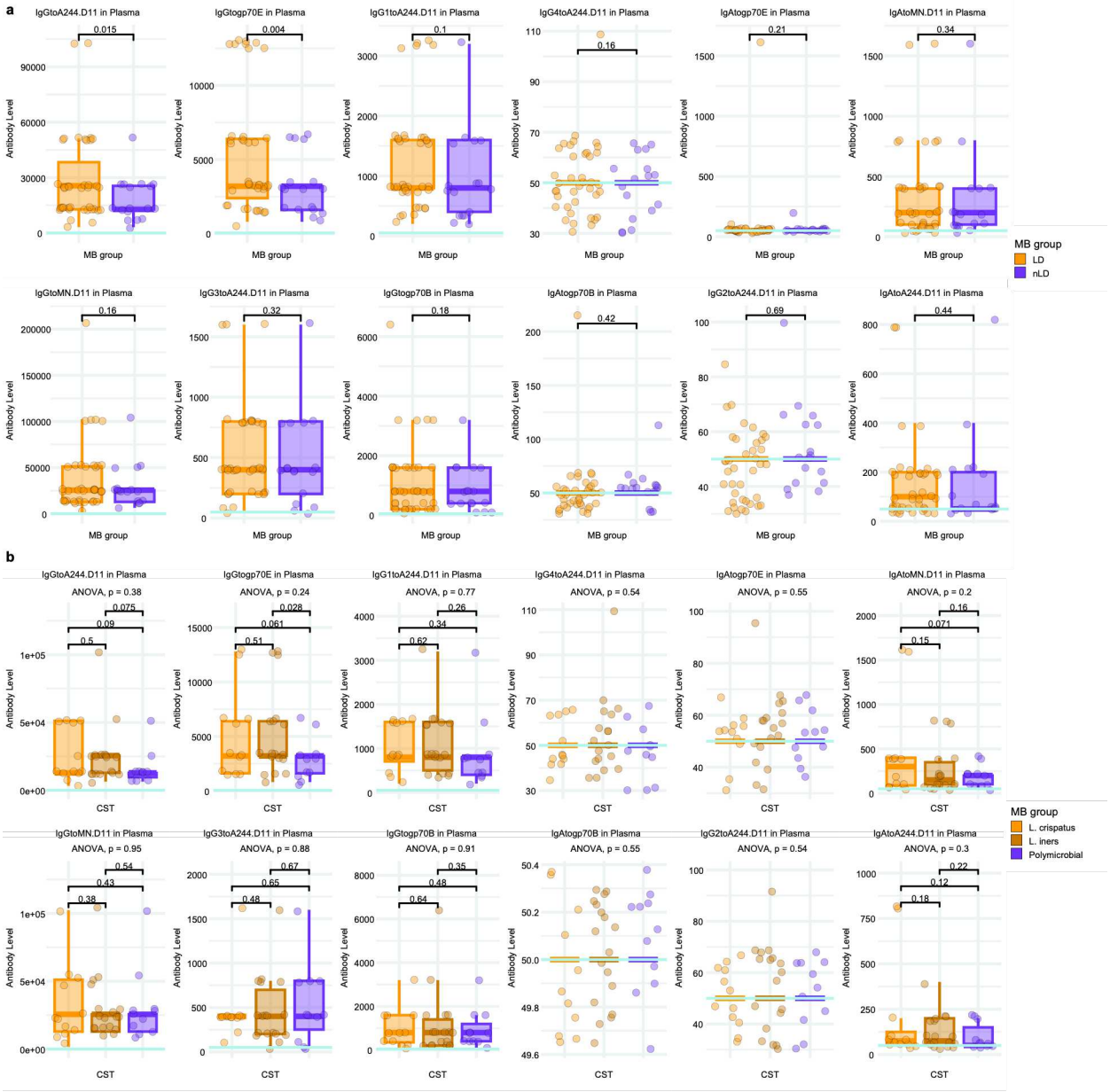
Curtis distances of taxa were used to identify microbiome composition. Annotation bars indicate LD status (LD or nLD), total *Lactobacillus* in the sample, whether the individual was in the vaccinated (active) or placebo group, visit, and dominant microbiome groups based on Pearson correlation (branches; *L. iners*, *L. crispatus*, and two polymicrobial groups).

Supplemental Figure 2



Significant antibodies analyses based on LD status or CST utilizing metagenomic characterizations. T-tests comparing antibody levels to LD status were performed for IgG-gp120 A244gD-D11 in plasma (A), IgG-gp70V1V2 92TH023 in plasma (B), and IgG-gp120 A244gD-D11 in mucosa (C). The LD participant group (orange) had more medium to high responders in all three antibodies compared to nLD (purple). The same comparisons are shown stratified based on CST status across the three antibodies (D-F).

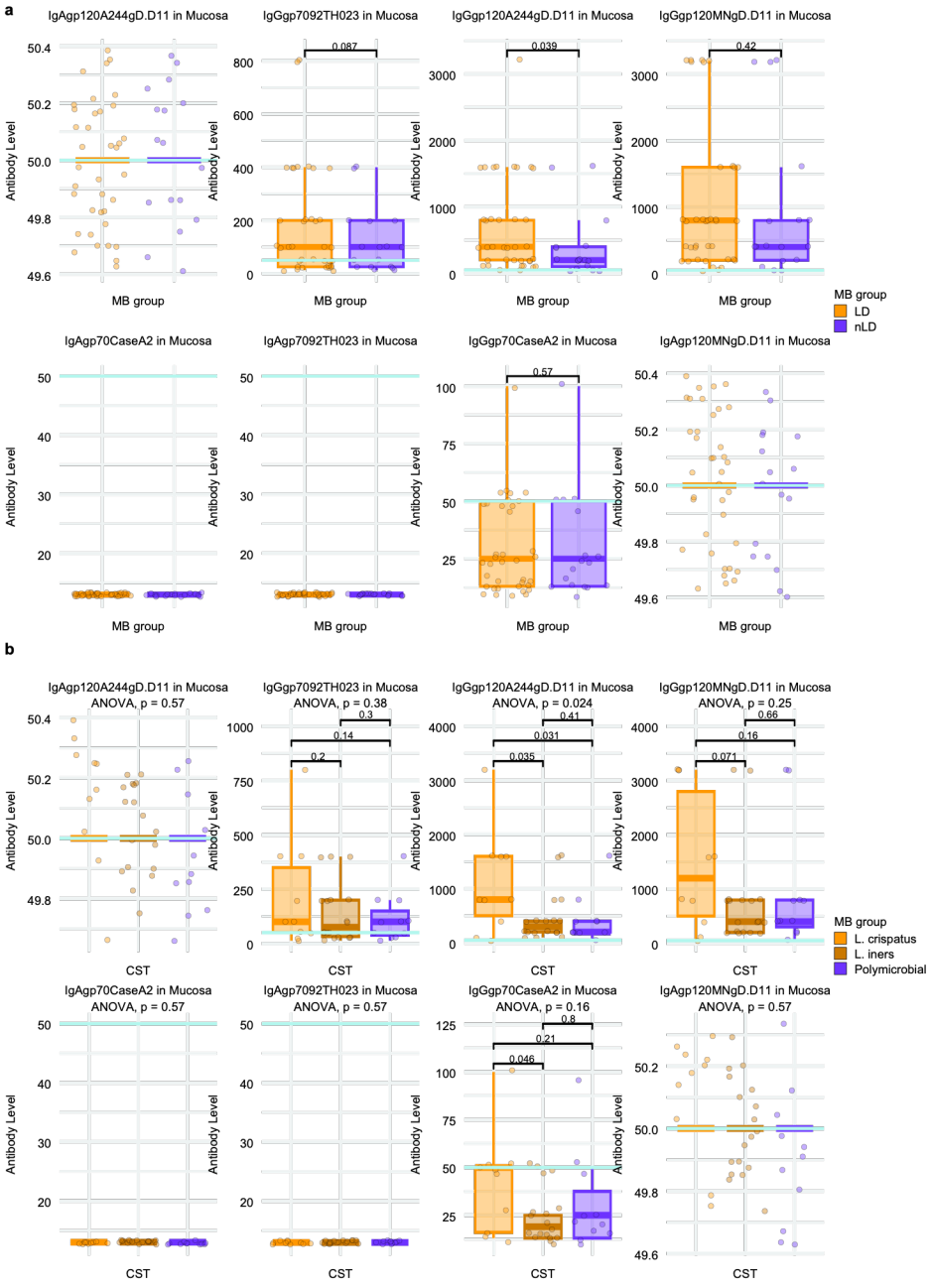
768 Supplemental Figure 3



769

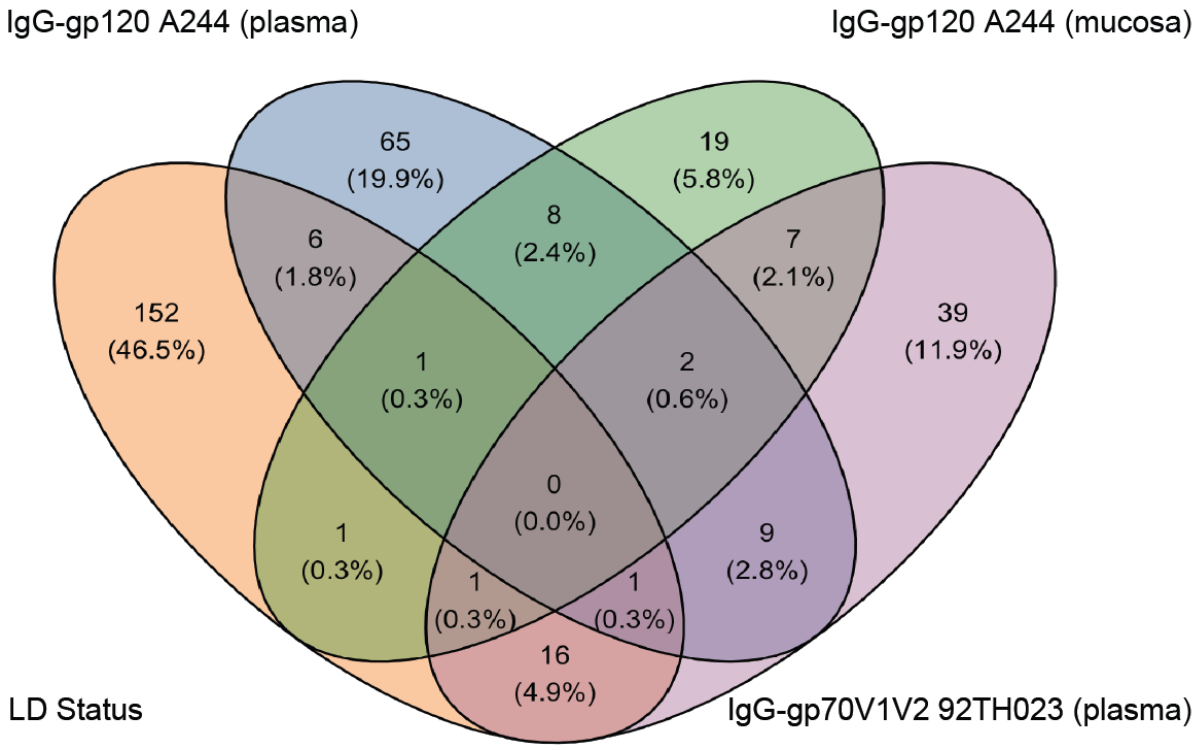
Association analyses with LD status or CST across all measured antibodies in plasma. T-tests comparing antibody levels to LD status were performed for all evaluated antibodies in plasma (A). The same statistical analyses are also performed based on CST stratifications (B).

Supplementary Figure 4



Association analyses with LD status or CST across all measured antibodies in mucosa. T-tests comparing antibody levels to LD status were performed for all evaluated antibodies in mucosa (A). The same statistical analyses are also performed based on CST stratifications (B).

Supplemental Figure 5



Differentially regulated proteins in overlapping significance groups. Comparison of differentially expressed proteins across stratified groups, showing shared and unique hits in a Venn diagram.

Consortia

The RV306 study group

Punnee Pitisuttithum[8], Jittima Dhitavat[8], Benjaluck Phonrat[8], Supat Chamnanchanunt[8], Arom Pitisuttithum[8], Kessuda Khowsroy[8], Sorachai Nitayaphan[6,12], Narongrid Sirisopana[12], Chirapa Eamsila[12], Wanlaya Lapwech[12], Prapaporn Savaraj[12], Siriluck Teerachia[12], Suwat Chariyalertsak[7], Natthapol Kosashunhanan[7], Nuntisa Chotirosniramit[7], Oranitcha Kaewthip[7], Taweewat Supindham[7], Wathee Sithi[7], Patcharaphan Sugandhavesa[7], Kittipong Rungruengthanakit[7], Kanlaya Wongworapat[7], Piyathida Sroysuwan[7], Boonlure Pruenglampoo[7], Praphan Phanuphak[13], Nittaya Phanuphak[13], Thep Chalermchai[13], James L.

K. Fletcher[13], Eugene Kroon[13], Nipat Teeratakulpisarn[13], Nitiya Chomchey[13], Putthachard Saengtawan[13], Jaranit Kaewkungwal[14], Pawinee Jarujareet[14], Robert J. O'Connell[6], Nicos Karasavvas[6], Alexandra Schuetz[3,6,8], Kirsten Smith[6], Siriwat Akapirat[6], Chitraporn Karnasuta[6], Sirinan Madnote[6], Surawach Rittiroongrad[6], Jiraporn Puangkaew[6], Somsak Chantakulkij[6], Bessara Nuntapinit[6], Phiromrat Rakyat[6], Tanyaporn Wansom[6], Anant Phramtong[6], Rapee Trichavaroj[6], Bhubate Tongchanakarn[6], Hathairat Savadsuk[6], Sandhya Vasan[3,4], Nelson L. Michael[4], Jintanat Ananworanich[4], Jerome H. Kim[4], Merlin L. Robb[4], Leigh Anne Eller[4], Chiaka Nwoga[4], Elizabeth Heger[4], Jean-Louis Excler[4], Charla Andrews[4], Faruk Sinangil[15], Carter Lee[15], Donald Francis[15], James Tartaglia[16], Sanjay Phogat[16], Suchada Chinaworapong[17]

12. Royal Thai Army–Armed Forces Research Institute of Medical Sciences, Bangkok, Thailand

13. Thai Red Cross AIDS Research Centre, Bangkok, Thailand

14. Center of Excellence for Biomedical and Public Health Informatics (BIOPHICS), Faculty of Tropical Medicine, Mahidol University, Bangkok, Thailand

15. Global Solutions for Infectious Diseases (GSID), South San Francisco, CA, USA

16. Sanofi Pasteur, Swiftwater, PA, USA

17. US Army Medical Materiel Development Activity (USAMMDA), Fort Detrick, MD, USA

References:

1. Global HIV & AIDS statistics — Fact sheet | UNAIDS. https://www.unaids.org/en/resources/fact-sheet.

2. Hammer, S. M. *et al.* Efficacy Trial of a DNA/rAd5 HIV-1 Preventive Vaccine. *N. Engl. J. Med.* **369**, 2083 (2013).

3. Buchbinder, S. P. *et al.* Efficacy assessment of a cell-mediated immunity HIV-1 vaccine (the Step Study): a double-blind, randomised, placebo-controlled, test-of-concept trial. *Lancet* **372**, 1881 (2008).

4. Baden, L. R. *et al.* First-in-Human Randomized, Controlled Trial of Mosaic HIV-1 Immunogens Delivered via a Modified Vaccinia Ankara Vector. *J. Infect. Dis.* **218**, 633 (2018).

5. Borthwick, N. J. *et al.* Randomized phase I trial HIV-CORE 003: Depletion of serum amyloid P component and immunogenicity of DNA vaccination against HIV-1. *PLoS One* **13**, e0197299 (2018).

6. Keefer, M. C. *et al.* A phase I double blind, placebo-controlled, randomized study of a multigenic HIV-1 adenovirus subtype 35 vector vaccine in healthy uninfected adults. *PLoS One* **7**, (2012).

7. Karasavvas, N. *et al.* The Thai Phase III HIV Type 1 Vaccine Trial (RV144) Regimen Induces Antibodies That Target Conserved Regions Within the V2 Loop of gp120. *AIDS Res. Hum. Retroviruses* **28**, 1444 (2012).

8. Rerks-Ngarm, S. *et al.* Vaccination with ALVAC and AIDSVAX to prevent HIV-1 infection in Thailand. *N. Engl. J. Med.* **361**, 2209–2220 (2009).

9. Gholiof, M., Adamson-De Luca, E. & Wessels, J. M. The female reproductive tract microbiotas, inflammation, and gynecological conditions. *Frontiers in Reproductive Health* **4**, 963752 (2022).

10. Anahtar, M. N., Gootenberg, D. B., Mitchell, C. M. & Kwon, D. S. Cervicovaginal Microbiota and Reproductive Health: The Virtue of Simplicity. *Cell Host Microbe* **23**, 159–168 (2018).

11. Daniel Johannes Rönnqvist, P., Birgitta Forsgren-Brusk, U. & Elisabeth Grahn-Håkansson, E. Lactobacilli in the female genital tract in relation to other genital microbes and vaginal pH. *Acta Obstet. Gynecol. Scand.* **85**, 726–735 (2006).

12. Dong, M. *et al.* Interactions between microbiota and cervical epithelial, immune, and mucus barrier. *Front. Cell. Infect. Microbiol.* **13**, 1124591 (2023).

13. McClelland, R. S. *et al.* Evaluation of the association between the concentrations of key vaginal bacteria and the increased risk of HIV acquisition in African women from five cohorts: a nested case-control study. *Lancet Infect. Dis.* **18**, 554–564 (2018).

14. Vielfort, K., Sjölinder, H., Roos, S., Jonsson, H. & Aro, H. Adherence of clinically isolated lactobacilli to human cervical cells in competition with Neisseria gonorrhoeae. *Microbes Infect.* **10**, 1325–1334 (2008).

15. Stout, M. J. *et al.* Early pregnancy vaginal microbiome trends and preterm birth. *Am. J. Obstet. Gynecol.* **217**, 356.e1-356.e18 (2017).

16. Hyman, R. W. *et al.* Diversity of the vaginal microbiome correlates with preterm birth. *Reprod. Sci.* **21**, 32–40 (2014).

17. Cheu, R. K. *et al.* Altered Innate Immunity and Damaged Epithelial Integrity in Vaginal Microbial Dysbiosis. *Frontiers in reproductive health* **4**, (2022).

18. Masson, L. *et al.* Genital inflammation and the risk of HIV acquisition in women. *Clin. Infect. Dis.* **61**, 260–269 (2015).

19. Gosmann, C. *et al.* Lactobacillus-Deficient Cervicovaginal Bacterial Communities Are Associated with Increased HIV Acquisition in Young South African Women. *Immunity* **46**, 29–37 (2017).

20. Wang, Y. *et al.* Non-Lactobacillus-Dominant and Polymicrobial Vaginal Microbiomes Are More Common in Younger South African Women and Predictive of Increased Risk of Human Immunodeficiency Virus Acquisition. *Clin. Infect. Dis.* **76**, 1372–1381 (2023).

21. Haynes, B. F. *et al.* Immune-Correlates Analysis of an HIV-1 Vaccine Efficacy Trial. *New England Journal of Medicine* **366**, 1275–1286 (2012).

22. Prentice, H. A. *et al.* HLA class II genes modulate vaccine-induced antibody responses to affect HIV-1 acquisition. *Sci. Transl. Med.* **7**, (2015).

23. Lagos, R. *et al.* Effect of small bowel bacterial overgrowth on the immunogenicity of single-dose live oral cholera vaccine CVD 103-HgR. *J. Infect. Dis.* **180**, 1709–1712 (1999).

24. Isolauri, E., Joensuu, J., Suomalainen, H., Luomala, M. & Vesikari, T. Improved immunogenicity of oral D x RRV reassortant rotavirus vaccine by Lactobacillus casei GG. *Vaccine* **13**, 310–312 (1995).

25. De Vrese, M. *et al.* Probiotic bacteria stimulate virus-specific neutralizing antibodies following a booster polio vaccination. *Eur. J. Nutr.* **44**, 406–413 (2005).

26. Harris, V. C. *et al.* Effect of Antibiotic-Mediated Microbiome Modulation on Rotavirus Vaccine Immunogenicity: A Human, Randomized-Control Proof-of-Concept Trial. *Cell Host Microbe* **24**, 197-207.e4 (2018).

27. Oh, J. Z. *et al.* TLR5-mediated sensing of gut microbiota is necessary for antibody responses to seasonal influenza vaccination. *Immunity* **41**, 478–492 (2014).

28. Trama, A. M. *et al.* HIV-1 envelope gp41 antibodies can originate from terminal ileum B cells that share cross-reactivity with commensal bacteria. *Cell Host Microbe* **16**, 215–226 (2014).

29. Pitisuttithum, P. *et al.* RV306, an Evaluation of a 48 Week ALVAC-HIV AIDSVAX B/E Vaccination Regimen in Thailand: Participation Rates for Optional Specimen Collections. *AIDS Res. Hum. Retroviruses* **30**, A264–A264 (2014).

30. Costanzo, M. C. *et al.* ALVAC-HIV and AIDSVAX B/E vaccination induce improved immune responses compared with AIDSVAX B/E vaccination alone. *JCI Insight* **8**, e167664 (2023).

31. Pitisuttithum, P. *et al.* Late boosting of the RV144 regimen with AIDSVAX B/E and ALVAC-HIV in HIV-uninfected Thai volunteers: a double-blind, randomised controlled trial. *Lancet HIV* **7**, e238–e248 (2020).

32. van Manen, D. *et al.* Genome-Wide Association Scan in HIV-1-Infected Individuals Identifying Variants Influencing Disease Course. *PLoS One* **6**, e22208 (2011).

33. Alisjahbana, B. *et al.* Neutrophils and lymphocytes in relation to MMP-8 and MMP-9 levels in pulmonary tuberculosis and HIV co-infection. *J. Clin. Tuberc. Other Mycobact. Dis.* **27**, 100308 (2022).

34. Identification of human cysteine-rich secretory protein 3 (CRISP-3) as a matrix protein in a subset of peroxidase-negative granules of neutrophils and in the granules of eosinophils - PubMed. https://pubmed.ncbi.nlm.nih.gov/12223513/.

35. Liu, G. ping, Xiang, L. xin, Shao, T., Lin, A. fu & Shao, J. zhong. Stimulatory function of peroxiredoxin 1 in activating adaptive humoral immunity in a zebrafish model. *Dev. Comp. Immunol.* **84**, 353–360 (2018).

36. Stolbova, E. A. *et al.* Early Transcriptomic Signatures of Immune Response Modulation Following Antiretroviral Therapy in HIV-Infected Patients. *Int. J. Mol. Sci.* **26**, 10678 (2025).

37. Huda, M. N. *et al.* Stool Microbiota and Vaccine Responses of Infants. *Pediatrics* **134**, e362–e372 (2014).

38. Eloe-Fadrosh, E. A. *et al.* Impact of Oral Typhoid Vaccination on the Human Gut Microbiota and Correlations with S. Typhi-Specific Immunological Responses. *PLoS One* **8**, e62026 (2013).

39. Su, L. F., Kidd, B. A., Han, A., Kotzin, J. J. & Davis, M. M. Virus-Specific CD4+ Memory-Phenotype T Cells Are Abundant in Unexposed Adults. *Immunity* **38**, 373–383 (2013).

40. Campion, S. L. *et al.* Proteome-wide analysis of HIV-specific naive and memory CD4(+) T cells in unexposed blood donors. *J. Exp. Med.* **211**, 1273–1280 (2014).

41. Hagan, T. *et al.* Antibiotics-Driven Gut Microbiome Perturbation Alters Immunity to Vaccines in Humans. *Cell* **178**, 1313-1328.e13 (2019).

42. Ryan, F. J. *et al.* Bifidobacteria support optimal infant vaccine responses. *Nature* **641**, 456–464 (2025).

43. Harris, V. *et al.* Rotavirus vaccine response correlates with the infant gut microbiota composition in Pakistan. *Gut Microbes* **9**, 93–101 (2018).

44. Seong, H. *et al.* The gut microbiota modifies antibody durability and booster responses after SARS-CoV-2 vaccination. *J. Transl. Med.* **22**, (2024).

45. Antunes, K. H. *et al.* Microbiota-derived acetate protects against respiratory syncytial virus infection through a GPR43-type 1 interferon response. *Nat. Commun.* **10**, (2019).

46. Bradley, K. C. *et al.* Microbiota-Driven Tonic Interferon Signals in Lung Stromal Cells Protect from Influenza Virus Infection. *Cell Rep.* **28**, 245-256.e4 (2019).

47. Elizaldi, S. R. *et al.* Rectal Microbiome Composition Correlates with Humoral Immunity to HIV-1 in Vaccinated Rhesus Macaques. *mSphere* **4**, (2019).

48. Tarabichi, Y. *et al.* The administration of intranasal live attenuated influenza vaccine induces changes in the nasal microbiota and nasal epithelium gene expression profiles. *Microbiome 2015 3:1* **3**, 74- (2015).

49. Ng, S. C. *et al.* Gut microbiota composition is associated with SARS-CoV-2 vaccine immunogenicity and adverse events. *Gut* **71**, 1106–1116 (2022).

50. Giraldo, P. C. *et al.* Relationship between Papillomavirus vaccine, vaginal microbiome, and local cytokine response: an exploratory research. *Brazilian Journal of Microbiology* **52**, 2363 (2021).

51. Eloe-Fadrosh, E. A. *et al.* Impact of oral typhoid vaccination on the human gut microbiota and correlations with s. Typhi-specific immunological responses. *PLoS One* **8**, (2013).

52. Sanjabi, S., Oh, S. A. & Li, M. O. Regulation of the Immune Response by TGF-β: From Conception to Autoimmunity and Infection. *Cold Spring Harb. Perspect. Biol.* **9**, a022236 (2017).

53. Yang, Y., Wang, Y., Jin, X. & He, W. Single-cell RNA-sequencing reveals cellular heterogeneity and immune microenvironment characteristics between ocular adnexal mucosa-associated lymphoid lymphoma and IgG4−related ophthalmic disease. *Front. Immunol.* **16**, 1508559 (2025).

54. He, J. Y. *et al.* Dysregulation of CD4+ and CD8+ resident memory T, myeloid, and stromal cells in steroid-experienced, checkpoint inhibitor colitis. *J. Immunother. Cancer* **12**, e008628 (2024).

55. Wang, M. *et al.* High-throughput single-cell profiling of B cell responses following inactivated influenza vaccination in young and older adults. *Aging (Albany NY)* **15**, 9250 (2023).

56. Herrero-Cervera, A., Soehnlein, O. & Kenne, E. Neutrophils in chronic inflammatory diseases. *Cellular & Molecular Immunology 2022 19:2* **19**, 177–191 (2022).

57. Klatt, N. R. *et al.* Vaginal bacteria modify HIV tenofovir microbicide efficacy in African women. *Science (1979).* **356**, 938–945 (2017).

58. Chen, S., Zhou, Y., Chen, Y. & Gu, J. fastp: an ultra-fast all-in-one FASTQ preprocessor. *Bioinformatics* **34**, i884–i890 (2018).

59. Babraham Bioinformatics - FastQC A Quality Control tool for High Throughput Sequence Data. https://www.bioinformatics.babraham.ac.uk/projects/fastqc/.

60. Bolger, A. M., Lohse, M. & Usadel, B. Trimmomatic: a flexible trimmer for Illumina sequence data. *Bioinformatics* **30**, 2114–2120 (2014).

61. Langmead, B. & Salzberg, S. L. Fast gapped-read alignment with Bowtie 2. *Nat. Methods* **9**, 357–359 (2012).

62. Ma, B. *et al.* A comprehensive non-redundant gene catalog reveals extensive within-community intraspecies diversity in the human vagina. *Nat. Commun.* **11**, (2020).

63. Perkins DN, P. D. C. D. C. J. Probability-based protein identification by searching sequence databases using mass spectrometry data. *Electrophoresis* (1999).

64. Scaffold | Proteome Software. https://www.proteomesoftware.com/.

65. Johnson, W. E., Li, C. & Rabinovic, A. Adjusting batch effects in microarray expression data using empirical Bayes methods. *Biostatistics* **8**, 118–127 (2007).

66. Dobin, A. *et al.* STAR: ultrafast universal RNA-seq aligner. *Bioinformatics* **29**, 15–21 (2013).

67. Kim, D., Langmead, B. & Salzberg, S. L. HISAT: a fast spliced aligner with low memory requirements. *Nat. Methods* **12**, 357–360 (2015).

68. Anders, S., Pyl, P. T. & Huber, W. HTSeq--a Python framework to work with high-throughput sequencing data. *Bioinformatics* **31**, 166–169 (2015).

69. Langfelder, P., Mischel, P. S. & Horvath, S. When Is Hub Gene Selection Better than Standard Meta-Analysis? *PLoS One* **8**, e61505 (2013).

70. Dong, J. & Horvath, S. Understanding network concepts in modules. *BMC Systems Biology 2007 1:1* **1**, 24- (2007).

Supplementary Files

This is a list of supplementary files associated with this preprint. Click to download.

- supplementaltable1.csv
- supplmentaltable2.csv